Tracking Maximum Produced Water Treatment Efficiency Using a Variable Speed Coalescing Centrifugal Pump

Rune Husveg

Tracking Maximum Produced Water Treatment Efficiency Using a Variable Speed Coalescing Centrifugal Pump

Doctoral Dissertation for the Degree *Philosophiae Doctor (PhD)* at
the Faculty of Engineering and Science, Specialisation in Mechatronics

University of Agder
Faculty of Engineering and Science
2019

Doctoral Dissertation at the University of Agder 218
ISSN: 1504-9272
ISBN: 978-82-7117-917-5

Printed by Wittusen & Jensen
Oslo

Acknowledgments

This project has been a part of the Research Council of Norway's Industrial Ph.D. Scheme and was possible due to their financial support. I would like to thank the Research Council for supporting my project, with special thanks to the people responsible for the Industrial Ph.D. Scheme.

Typhonix AS has been a solid foundation, and I would like to thank for the funding and opportunity to carry out this project. Special thanks to Trygve Husveg and Niels van Teeffelen for being my industrial supervisors; you are walking and talking encyclopedias. Also, thanks to Olav Austbø for supporting me during the construction of the test rig.

I am grateful for the dynamic environment at the University of Agder, allowing me to peruse my topic of choice. Special thanks to Michael Rygaard Hansen and Morten Ottestad for willingly guiding me through this project, and for being my main-supervisor and co-supervisor, respectively.

Thanks to my family and friends for supporting me and for pretending to be interested in my research. Thanks also to my colleagues at the University of Agder; you have been a source of great inspiration, and your lively environment has kept me going through long hours.

Rune Husveg
Bryne, Norway
August 2018

Abstract

Produced water is the most significant by-product of petroleum production. Even though naturally occurring, the produced water poses substantial environmental impacts if not managed correctly, and it is often associated with large volumes and high handling costs.

Oil removal is one of the primary goals of produced water treatment. The efficiency of the treatment equipment is usually highly sensitive to the oil droplet's size. Generally, the larger the droplets, the better the separation. Due to the importance of large oil droplets, droplet breakup in process equipment such as pumps and valves should be kept to a minimum.

Recently, a novel coalescing multistage centrifugal pump has been introduced to particularly target produced water applications. This pump promotes droplet growth rather than breakage, and thereby increases the efficiency of downstream treatment equipment.

This thesis shows that the novel coalescing centrifugal pump can be actively controlled to maximize the efficiency of downstream produced water treatment equipment, using real-time process information and tracking techniques. A once-through test rig has been designed, built, and used to study the coalescing performance of the novel pump. The rig has also been used to study the characteristics and benefits of combining the coalescing pump with a deoiling hydrocyclone.

Perturb-and-observe (P&O)-algorithms have been developed and successfully implemented to actively control the pumping pressure and to continuously track the point of operation resulting in the highest downstream separation efficiency. The continuous tracking techniques have been compared to a model-prediction method, optimizing the pump operation based on upstream process information. In addition, the P&O-algorithms have been further improved by introducing a variable step size, and routines to avoid tracking failure.

In total, this project has resulted in a unique and novel utilization of emerging pump technology. Concerning operational control, the coalescing pump has been innovatively combined with existing produced water treatment equipment, utilizing the potential of the pump to maximize the treatment efficiency.

Publications

The following four papers are appended in the form they were published or submitted and will be referred to either as Paper A, Paper B, Paper C and Paper D, or as [1], [2], [3] and [4], respectively.

Paper A R. Husveg, T. Husveg, N. van Teeffelen, M. Ottestad, and M. R. Hansen. Performance of a Coalescing Multistage Centrifugal Produced Water Pump with Respect to Water Characteristics and Point of Operation. In *Proc. of the Produced Water Workshop*, Aberdeen, United Kingdom, June 2016.

Paper B R. Husveg, T. Husveg, N. van Teeffelen, M. Ottestad, and M. R. Hansen. Improving Separation of Oil and Water With a Novel Coalescing Centrifugal Pump. *SPE Production & Operations*, Preprint, 2018. SPE-188772-PA.

Paper C R. Husveg, T. Husveg, N. van Teeffelen, M. Ottestad, and M. R. Hansen. Automatic Operation and Control of a Novel Coalescing Centrifugal Pump for Improved Oil/Water Separation. Manuscript submitted for publication, 2018.

Paper D R. Husveg, T. Husveg, N. van Teeffelen, M. Ottestad, and M. R. Hansen. Variable Step Size P&O Algorithms for Coalescing Pump/Deoiling Hydrocyclone Produced Water Treatment System. Manuscript submitted for publication, 2018.

The following paper was written and published during the time of this project but is not included in the thesis.

Paper E R. Husveg, T. Husveg, N. van Teeffelen, M. Ottestad, and M. R. Hansen. Improving Separation of Oil and Water Using a Novel Coalescing Centrifugal Pump. In *Proc. of the Abu Dhabi International Petroleum Exhibition & Conference*, Abu Dhabi, United Arab Emirates, November 2017. SPE-188772-MS

Contents

List of Figures

List of Tables

Abbreviations

AC alternating current.

BAT best available technique.

BEP best environmental practice.

BTEX benzene, toluene, ethylbenzene and xylene.

BVSS basic variable step size.

CSS constant step size.

CV control valve.

DPT differential-pressure transmitter.

EIF environmental impact factor.

EU European Union.

FINS Factory Interface Network Service.

FT flow transmitter.

HMI human–machine interface.

HVSS hybrid variable step size.

MPPT maximum power point tracking.

NORM naturally-occurring radioactive material.

OPC Open Platform Communications.

P&O perturb-and-observe.

PAH polycyclic aromatic hydrocarbon.

PC personal computer.

PDR pressure-drop ratio.

PLC programmable logic controller.

PWC produced water characteristic.

rpm revolutions per minute.

TD Turner Design.

TVSS triggered variable step size.

VFD variable-frequency drive.

VSD variable-speed drive.

VSS variable step size.

Nomenclature

A area.

$a_{\mathbf{r}}$ radial acceleration.

$C_{\mathbf{d}}$ downstream oil concentration.

$C_{\mathbf{d}}^{(\mathbf{min})}$ lowest measured C_{d}.

$C_{\mathbf{d,n}}$ current C_{d}.

$C_{\mathbf{d,n\text{-}1}}$ previous C_{d}.

$C_{\mathbf{in}}$ hydrocyclone inlet oil concentration.

$C_{\mathbf{u}}$ upstream oil concentration.

$C_{\mathbf{uf}}$ hydrocyclone underflow oil concentration.

$\bar{C}_{\mathbf{d,n}}$ mean of $C_{\mathrm{d,n}}$ and $C_{\mathrm{d,n\text{-}1}}$.

D pipe diameter.

d droplet diameter.

$d_{\mathbf{50}}$ hydrocyclone cut-size.

$d_{\mathbf{lim}}$ limit droplet diameter.

$d_{\mathbf{max}}$ maximum stable droplet diameter.

$d_{\mathbf{v50}}$ volume median droplet diameter.

$d_{\mathbf{v50,u}}$ upstream d_{v50}.

$E_{\mathbf{HC}}$ hydrocyclone separation efficiency.

$E_{\mathbf{HC}}@\Delta p_{\mathbf{opt}}$ hydrocyclone separation efficiency at the optimal pumping pressure.

F hydrocyclone flow split.

$F_{\mathbf{d}}$ Stokes' drag force.

$F_{\mathbf{g}}$ excess force due to difference between weight and buoyancy.

$F_{\mathbf{H}}$ cumulative droplet size distribution.

f friction factor.

G hydrocyclone migration probability.

g gravitational acceleration.

H volumetric droplet size distribution.

$H_{\mathbf{in}}$ hydrocyclone inlet H.

$H_{\mathbf{uf}}$ hydrocyclone underflow H.

h energy dissipation per unit mass.

K tuning parameter.

L pipe segment length.

n current iteration number.

$p_{\mathbf{d}}$ downstream pressure.

$p_{\mathbf{m}}$ midstream pressure.

$p_{\mathbf{o}}$ overflow pressure.

$p_{\mathbf{u}}$ upstream pressure.

$p_{\mathbf{u}}^{\mathbf{SP}}$ set-point p_{u}.

Q flow rate.

$Q_{\mathbf{in}}$ hydrocyclone inlet Q.

$Q_{\mathbf{o}}$ hydrocyclone overflow Q.

$Q_{\mathbf{s}}$ sample Q.

$Q_{\mathbf{s}}^{\mathbf{SP}}$ set-point Q_{s}.

$Q_{\mathbf{u}}$ upstream Q.

$Q_{\mathbf{u}}^{\mathbf{SP}}$ set-point Q_{u}.

R_1 sum of $\delta_{\Delta \mathrm{p}}$.

R_1' rescaled R_1.

R_2 sum of $C_{\mathrm{d}} \cdot \Delta t$.

R_2' rescaled R_2.

r distance from cyclone center (radius).

t time.

u mean flow velocity.

$u_{\mathbf{PW}}$ produced water flow velocity.

$u_{\mathbf{s}}$ sample flow velocity.

V volume.

$v_{\mathbf{T}}$ tangential velocity.

$v_{\mathbf{t}}$ terminal velocity.

$\Delta d_{\mathbf{v50}}{}^{(\%)}$ percentage change of d_{v50}.

$\Delta p_{\mathbf{avg}}$ average optimal pumping pressure.

$\Delta p_{\mathbf{cp}}$ coalescing pump pumping pressure.

$\Delta p_{\mathbf{cp}}^{\mathbf{SP}}$ set-point Δp_{cp}.

$\Delta p_{\mathbf{cp,n}}$ current Δp_{cp}.

$\Delta p_{\mathbf{cp,n\text{-}1}}$ previous Δp_{cp}.

$\Delta p_{\mathbf{opt}}$ optimal pumping pressure.

$\Delta p_{\mathbf{pre}}$ model predicted optimal pumping pressure.

$\Delta p_{\mathbf{uf}}$ hydrocyclone underflow pressure drop.

$\Delta p_{\mathbf{v}}$ valve pressure drop.

Δt step time.

$\delta_{\mathbf{\Delta p}}$ pumping pressure step size.

$\delta_{\mathbf{\Delta p}}^{\mathbf{(max)}}$ maximum $\delta_{\Delta \mathrm{p}}$.

$\delta_{\mathbf{\Delta p}}^{\mathbf{(min)}}$ minimum $\delta_{\Delta \mathrm{p}}$.

$\delta_{\mathbf{\Delta p,n}}$ current $\delta_{\Delta \mathrm{p}}$.

$\delta_{\mathbf{\Delta p,n\text{-}1}}$ previous $\delta_{\Delta \mathrm{p}}$.

ε energy dissipation rate per unit mass.

$\mu_{\mathbf{o}}$ oil dynamic viscosity.

$\mu_{\mathbf{w}}$ water dynamic viscosity.

$\rho_{\mathbf{c}}$ continuous phase density.

$\rho_{\mathbf{o}}$ oil density.

$\rho_{\mathbf{w}}$ water density.

σ interfacial tension.

$\varphi_{\mathbf{PDR}}$ hydrocyclone pressure drop ratio.

$\varphi_{\mathbf{PDR}}^{\mathbf{SP}}$ set-point φ_{PDR}.

$\%V_{\mathbf{d<d_{lim}}}$ volume fraction of droplet smaller than d_{lim}.

$\%V_{\mathbf{d>d_{lim}}}$ volume fraction of droplet larger than d_{lim}.

Chapter 1

Introduction

In this thesis, the coalescing performance of a novel centrifugal pump is studied and actively controlled to improve the efficiency of downstream produced water treatment equipment. Produced-water is water brought up to the surface during oil and gas production. This water contains toxic and harmful substances and must be treated before it can be discharged into the environment or re-injected into the well [5].

Oil removal is one of the primary goals of produced water treatment, and the efficiency of the treatment equipment is usually sensitive to the droplet's size. Generally, the larger the droplets, the better the separation [6]. Due to the importance of large oil droplets, droplet breakup in process equipment should be kept to a minimum [7, 8]. The novel pump is a coalescing multistage centrifugal pump particularly targeting produced water applications. Generally, this pump promotes droplet growth rather than breakage, which can increase the efficiency of the downstream treatment equipment [9].

In the following introduction, the estimated volume of water produced globally and on the Norwegian continental shelf are presented. Next, the produced water treatment system considered in this project is introduced. In addition, there is a state-of-the-art review of deoiling hydrocyclones and pumps in produced water applications, and a brief introduction of the novel coalescing pump. Furthermore, the considered control strategies, the main hypothesis, the project objectives and the thesis outline are presented.

1.1 Background

The OSPAR Recommendation 2001/1 defines produced water as

> water which is produced in oil and/or gas production operations and includes formation water, condensation water and re-produced injection water; it also includes water used for desalting oil. [10]

Produced water is the most significant by-product of petroleum production [5]. Because of the large volume and high handling costs, managing produced water is a vital issue. Even though naturally occurring, produced water pose substantial environmental impacts if not managed correctly [11].

On a worldwide basis, the current estimated produced water-to-oil ratio is between 3 : 1 [5] and 4 : 1 [12], and rising. The ratio increases as old fields mature, at the same time as it is being restrained by better management methods and the introduction of new fields [5]. On the Norwegian continental shelf, some older fields may produce up to 90 % water [13].

Globally, around 250 million barrels of water are produced daily, and more than 40 % of this is discharged into the environment [5, 14]. In 2012, 164 million m^3 produced water was in total reported for the Norwegian continental shelf, and at least 130 million m^3 of this was discharged into the environment [15]. In 2015, these numbers were 186.7 million m^3 water produced and 148.2 million m^3 discharged [16]. The volume of produced water was in 2015 expected to increase until 2017/18, before starting to decline [15]. The portion of produced water discharged into the environment is expected to decrease to around 60 % by 2020, and to continue declining [15].

The average concentration of oil discharged on the Norwegian continental shelf was from 2006 to 2015 between 9 to 12.5 mg/l, where the concentration increased slightly throughout this period [15]. On a monthly average, most fields were operated with discharges below the limit of 30 mg/l [15].

As the portion of produced water increases, and fields are kept in operation for extended periods of time, continuous improvement of the water treatment is essential to avoid harming the environment. This project aims at improving the water treatment by utilizing the potential of emerging technologies, and innovatively combine them with existing technologies and systems.

1.2 Considered system

In the North Sea, three-phase separators are normally used to separate most of the produced water and gas from the crude oil [17]. Subsequently, in combination with other treatment technologies, deoiling hydrocyclones are often used to remove the remaining dispersed oil from the produced water [17]. In facilities with low process pressure, pumps may be used to increase the pressure and to maintain it above a certain level [7].

Figure 1.1 sketches an imagined produced water treatment facility containing the coalescing pump, a deoiling hydrocyclone, and downstream control valves. Water brought up from the reservoir is separated from the produced oil and gas in the three-phase

separator. The separated oil and gas then flow toward their designated treatment facilities, while the produced water flows toward the considered system. In the considered system, indicated by the gray dotted square, the produced water is treated using the hydrocyclone which is boosted by the coalescing pump. After separation, the oil-enriched reject stream is routed toward the oil treatment facility, whereas the cleaned water is routed toward further treatment, here exemplified by a degassing vessel.

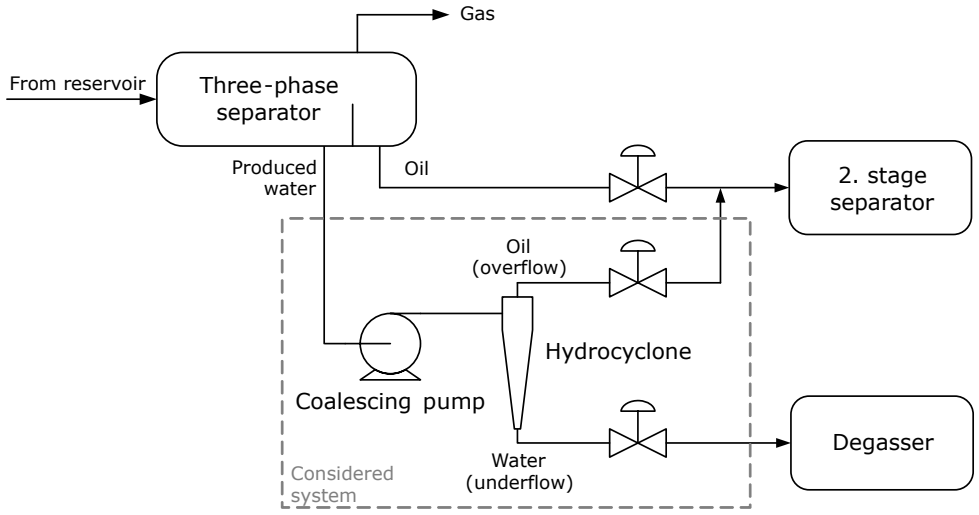

Figure 1.1: Sketched produced water treatment facility containing the coalescing pump, a hydrocyclone, and downstream control valves.

The considered system will be used throughout this project to study the benefits of including and actively controlling the novel coalescing centrifugal pump.

1.3 State-of-the-art

This section introduces deoiling hydrocyclones, pumps in produced water applications, and the novel coalescing pump.

1.3.1 Deoiling hydrocyclones

Related to petroleum processing, hydrocyclones are often divided into *deoilers*, *dewaterers* and *desanders*. Desanding hydrocyclones are solid-liquid separators, separating produced sand from crude oil and water. Dewatering and deoiling hydrocyclones are liquid-liquid separators. The former is used to dehydrate crude oil, while the latter removes residual oil from the produced water [7]. This project will be focusing on deoiling hydrocyclones for produced water applications.

Deoiling hydrocyclones have been successfully installed on platforms since the early 1980s [18, 19], as exemplified by [20, 21, 22]. Today, they are one of the most commonly

used technologies on the Norwegian continental shelf [13]. Hydrocyclones are usually chosen due to their simplicity, compactness, robustness, and low manufacturing and maintenance cost [18]. Whether hydrocyclones are installed vertically or horizontally does not influence the separation performance [7]. However, they may get clogged or require cleaning, and are often flushed regularly [15]. To increase the capacity, several hydrocyclone units (also called liners) are typically installed in parallel within a single pressure-vessel [8, 21]. The pressure-vessel also allows the liners to be made of relatively thin-walled material. Blanks, later to be replaced by liners, can be installed in the vessel to adjust the capacity as the water production rates change [8].

Hydrocyclones are usually controlled by the downstream control valves, and the system includes both flow rate and flow split control [8, 19, 20]. The underflow control valve (water outlet, Figure 1.1) is normally used to maintain a pre-set fluid level in the three-phase separator, thereby controlling the flow rate. The overflow control valve (oil outlet, Figure 1.1) controls the flow split within the hydrocyclone. Here, the control structure is usually based on the pressure-drop ratio (PDR) between the two outlet pressures relative to the inlet pressure [23], employing an approximately linear relationship between the PDR and the flow split. Recent work has been done to develop a direct efficiency control for deoiling hydrocyclones [24, 25]. However, the project presented in this thesis will employ the standard flow rate and flow split control.

1.3.2 Pumps in produced water applications

Following the success of deoiling hydrocyclones, it became increasingly appealing to look for solutions to employ pumps at fields or locations in the process with insufficient feed pressure. Early attempts were conducted with little knowledge about pumping and valve arrangements suitable for use with hydrocyclones [20].

To assist in the development, the use of droplet size analysis to evaluate separators and other production equipment was investigated [26]. As a part of this survey, seven different pumps were tested and rated based on droplet breakage. The pumps represented five different generic types and were ranked from 1 to 5, where one was the best, and five was the poorest. The following ranking was presented: (1) progressive cavity pumps, (2) twin lobe pumps, (3) sliding rotary vane pumps, (4) single stage centrifugal pumps, and (5) twin screw pumps.

In the light of the initial attempts to use hydrocyclones on low-pressure sources, and based on the above ranking, a study was conducted to determine the most suitable pumping system [27]. The study showed that a progressive cavity pump could be successfully combined with deoiling hydrocyclones.

In the search for a simpler and more cost-effective alternative, it was found that

centrifugal pumps could be used by limiting the pumping pressure and correctly selecting the involute type, diameter, and revolutions per minute (rpm) [28]. A re-cycle line was installed downstream of the hydrocyclone, recycling parts of the flow upstream of the pump, and allowing the pump and hydrocyclone to operate at a constant flow rate [28].

Summarizing the development, it was stated that pump selection and operation are equally important [7]. It was also stated that positive displacement pumps could provide low droplet breakage, but typically require more maintenance than centrifugal pumps [7]. Centrifugal pumps may also provide reduced droplet breakage when properly sized and correctly used [7]. A centrifugal pump with a closed impeller design should be selected and operated with a hydraulic efficiency above 70 % and a maximum speed of 1800 rpm [7]. Furthermore, both single-stage and multi-stage centrifugal pumps may be used, where a single stage pump should not provide a pumping pressure above 80 psig [7]. The flow rate in pumped hydrocyclone systems should be controlled by re-cycle loops or by variable-speed drives (VSDs) [7].

Similar recommendations have later been presented by other investigators, recommending a shaft speed below 1800 rpm, hydraulic efficiency above 60 %, large impeller diameters, over-sized discharge nozzle for slow discharge speed, pumping pressure below 50 psi per stage, and a specific speed below 700 [29]. Replacing constant speed operation by installing VSDs has also been recommended to reduce the droplet breakage [6].

1.3.3 Novel coalescing pump

In recent years, a coalescing multistage centrifugal pump for produced water applications has been introduced [9]. This pump increases, rather than reduces, the size of the dispersed oil droplets by promoting droplet-droplet coalescence. Figure 1.2 shows an illustration of the pump internals, where the main features are (1) the low-shear pumping stages, (2) the coalescing impeller configuration, and (3) the coalescing diffuser structures.

The coalescing pump was introduced by presenting prototype test results [9]. The prototype testing featured, among other investigations, a comparative study including the coalescing pump and two typical produced water pump types. In the study, all pumps were operated at the best efficiency point, and the results highlighted how the novel pump increased the volume median droplet diameter (d_{v50}) for various upstream produced water characteristics (e.g., the upstream droplet size distribution, oil concentration, and oil type).

Although only presented in internal reports, it has also been observed that the coalescing effect is affected by the point of operation (i.e., the combination of pumping pressure and flow rate). As a result, it was theorized that the point of operation could be continuously adjusted to optimize the coalescence and to maximize the downstream

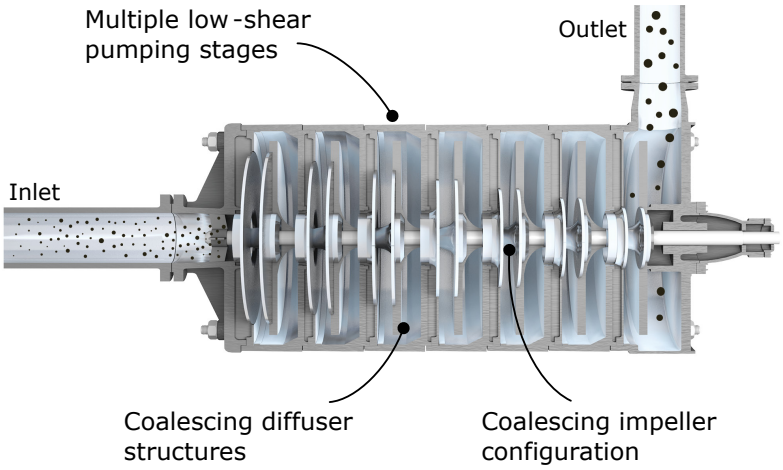

Figure 1.2: Illustration of the novel coalescing multistage centrifugal pump internals.

separation efficiency. Downstream control valves may be employed to account for the varying pressure and an online oil-in-water analyzer included for process feedback. In the work of this thesis, this concept will be further investigated by employing various control strategies.

1.4 Considered control strategies

For a centrifugal pump, the pumping pressure is governed by both the flow rate and the rotational speed [30]. In the considered system (Figure 1.1), the flow rate is controlled by the underflow control valve. The pumping pressure is therefore controlled by adjusting the rotational speed of the pump. For the considered control strategies, the rotational speed is continuously adjusted by a variable-frequency drive (VFD), employing conventional closed-loop feedback control, as shown in Figure 1.3.

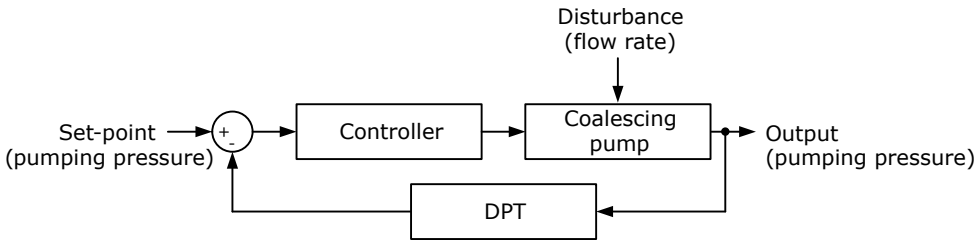

Figure 1.3: Closed-loop feedback control of the coalescing centrifugal pump.

Figure 1.3 shows a block diagram of the coalescing-pump control. The input of the pump block is the rotational speed, while the output is the resulting pumping pressure. The varying flow rate is included as a disturbance. The block diagram also includes the closed-loop feedback controller, whose input is the error between the desired pumping

pressure (set-point) and the actual pumping pressure (feedback); the latter is measured by a differential-pressure transmitter (DPT).

By including an oil-in-water analyzer, the approach is to use process feedback information to continuously optimize the coalescing effect of the pump, by adjusting the pumping pressure. As long as (1) the pump is operated within a predetermined envelope, (2) the stepwise pumping pressure changes are controlled, and (3) the downstream valves are sufficiently fast, the pressure changes can be introduced without affecting the overall process plant.

Following are descriptions of the considered control strategies, characterized by the location of the oil-in-water analyzer. Figure 1.4 sketches the instrumentation and indicates potential analyzer locations.

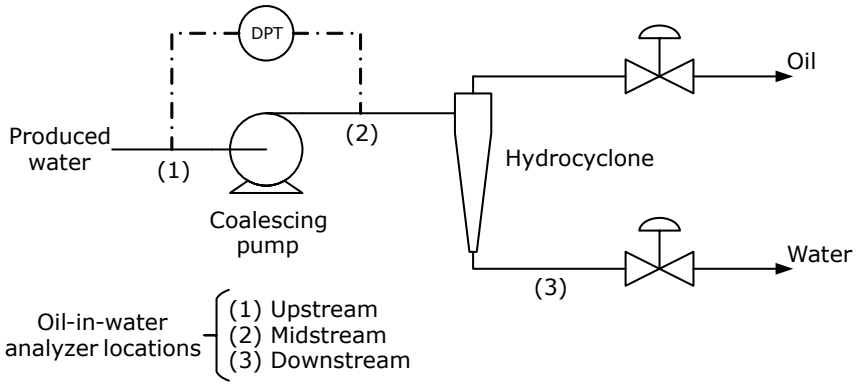

Figure 1.4: Sketch of the considered system, instrumentation, and potential placings of the oil-in-water analyzer.

The oil-in-water analyzer may be placed in the *upstream* position, measuring the characteristics of the produced water upstream of the coalescing pump. Alternative placings are the *midstream* position, between the pump and the hydrocyclone, or the *downstream* position, downstream of the hydrocyclone. Figure 1.5 expands the block diagram of Figure 1.3 to include the characteristics of the produced water throughout the considered system.

In the figure, the upstream produced water characteristics are added as a disturbance to the coalescing pump block, while the midstream produced water characteristics are included as output. The downstream produced water characteristics are included as an output of the hydrocyclone, characterized by the resulting oil concentration. Various versions of this block diagram will be presented for the alternative analyzer placings, including the considered control strategies.

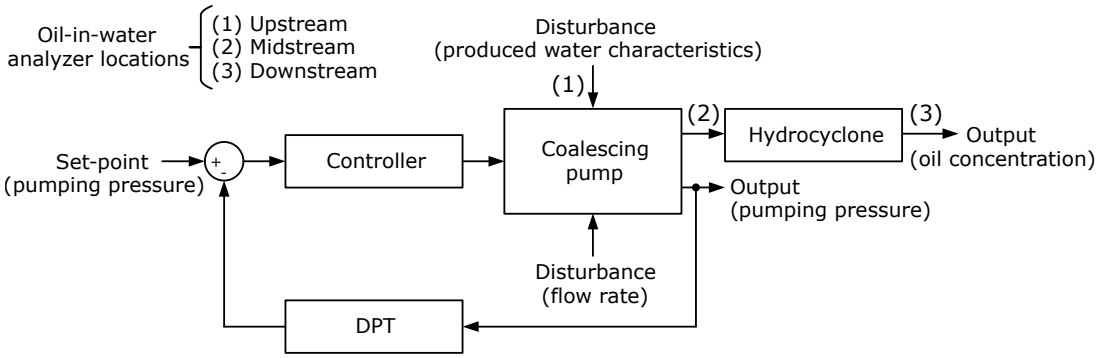

Figure 1.5: Expanded block diagram of the considered system.

1.4.1 Oil-in-water analyzer position 1: Upstream

An oil-in-water analyzer placed in the *upstream* position can provide information such as oil concentration and pump inlet droplet size distribution. Figure 1.6 shows a block diagram of the considered system, including an analyzer in the *upstream* position.

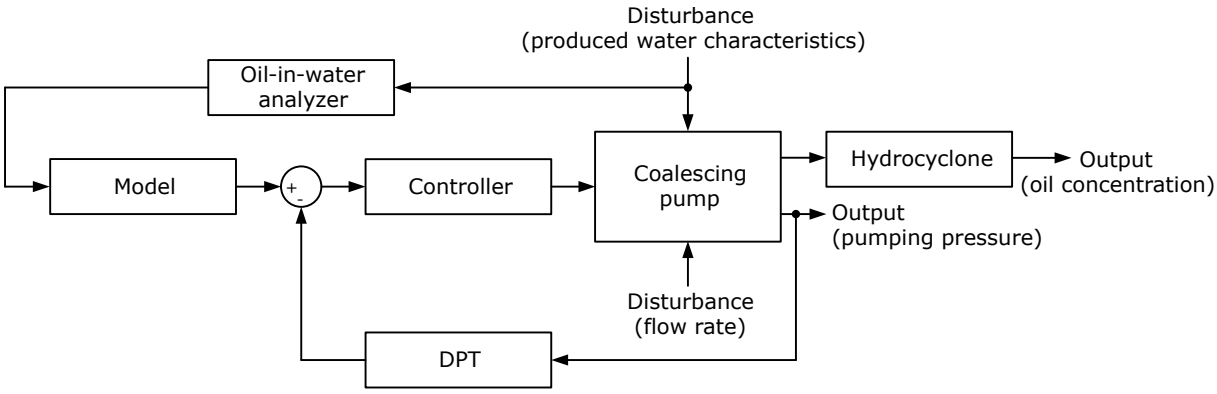

Figure 1.6: Block diagram of the considered system with an oil-in-water analyzer in the *upstream* position.

By having a model of the coalescing pump and hydrocyclone separation, the upstream measurements can be used to predict the optimal pumping pressure. The model-predicted pumping pressure will, in turn, be used as set-point for the closed-loop pumping pressure controller. If changes in the upstream produced water characteristics occur, the model will immediately renew the predicted optimal pumping pressure, and coalescing pump will be adjusted accordingly.

1.4.2 Oil-in-water analyzer position 2: Midstream

Placed in the *midstream* position, the oil-in-water analyzer can be used to measure the midstream droplet size distribution. Figure 1.7 shows a block diagram of the considered system, including an analyzer in the *midstream* position.

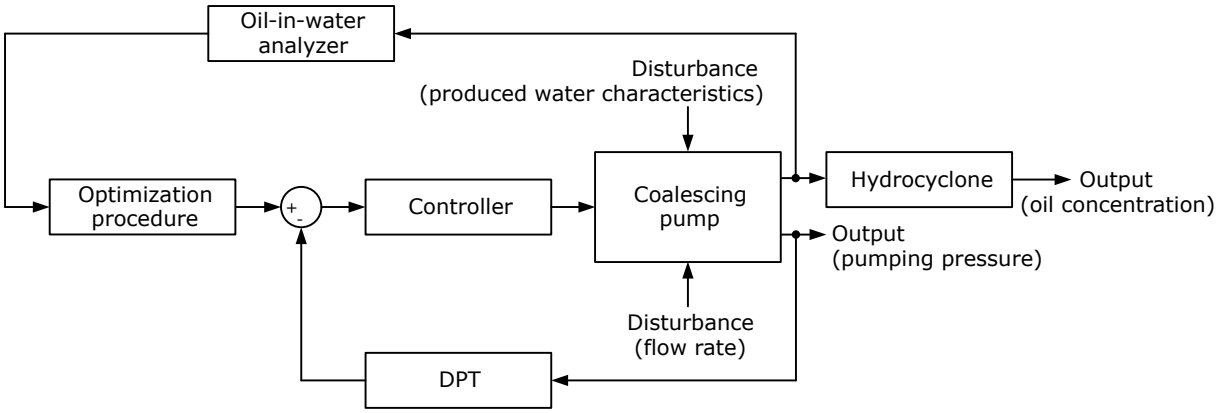

Figure 1.7: Block diagram of the considered system with an oil-in-water analyzer in the *midstream* position.

Having a model of the hydrocyclone separation, and therefore knowing the features of an advantageous inlet droplet size distribution, the pumping pressure can be optimized based on measurements of the resulting midstream droplet size distribution. This setup does not require a model of the coalescing pump; however, an optimization procedure is required. The optimization procedure should systematically adjust the pumping pressure, and thereby approach the point of operation resulting in the most advantageous midstream droplet size distribution.

1.4.3 Oil-in-water analyzer position 3: Downstream

An oil-in-water analyzer in the *downstream* position can provide information about the actual product, i.e., the cleaned water. Figure 1.8 shows a block diagram of the considered system, including an analyzer in the *downstream* position.

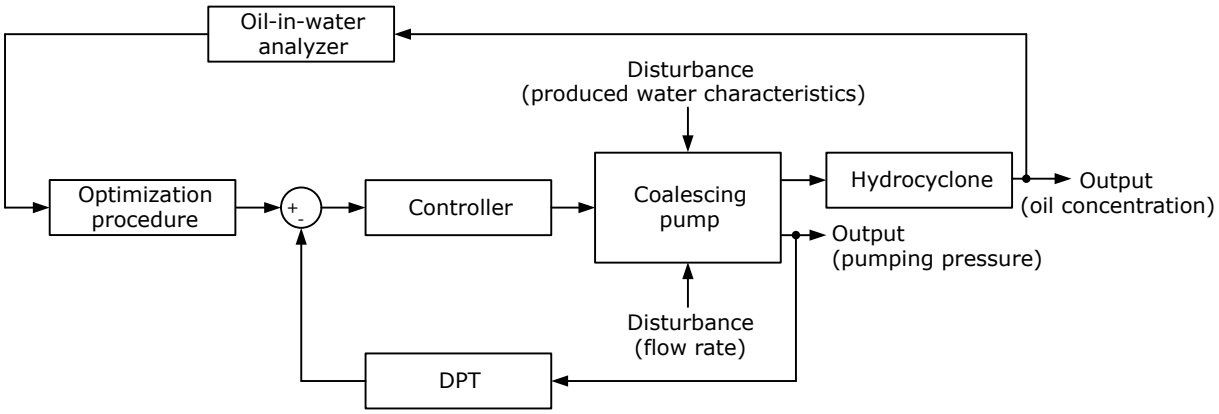

Figure 1.8: Block diagram of the considered system with an oil-in-water analyzer in the *downstream* position.

Having an optimization procedure, trends in the resulting oil concentration can be

used to approach the optimal pumping pressure without requiring any prior information or model of neither the coalescing pump nor the hydrocyclone.

1.4.4 P&O-algorithms

Placing the oil-in-water analyzer in the *midstream* or *downstream* position requires an optimization procedure. Related to power generation, maximum power point tracking (MPPT) is a technique commonly used to maximize the power generation continuously [31]. Examples of applications are photo-voltaic systems [32] and wind energy conversion systems [33]. Several algorithms and techniques are developed to conduct the MPPT; amongst the most commonly used are perturb-and-observe (P&O)-algorithms [31, 32].

Figure 1.9 shows general schematics of a P&O-algorithm. The algorithm is characterized by first performing a process variable change (perturb), before measuring the effect (observe). Based on the observed effect, the algorithm determines the following process variable change. When the optimal variable value has been found, the algorithm encircles this value until any process changes occur that may shift the optimal value.

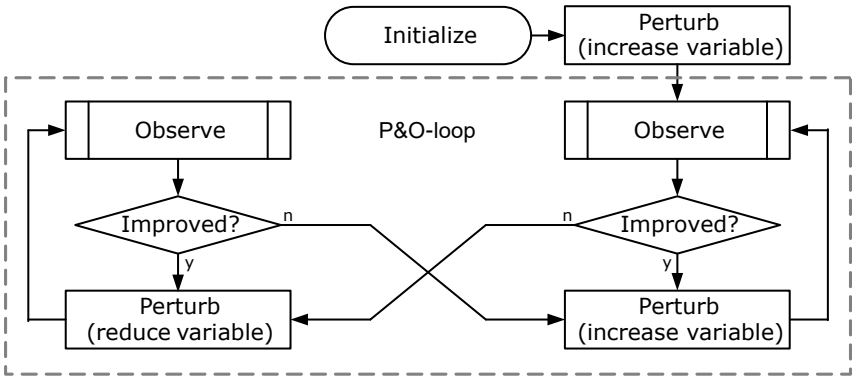

Figure 1.9: General schematics of a P&O-algorithm.

P&O-algorithms are often chosen because of their simple construction and ease of implementation [31, 32]. However, drawbacks are the continuous perturbations and oscillations around the maximum power point [31, 32]. Generally, constant step size P&O-algorithms introduce a trade-off when choosing the size of the step [34]. On the one hand, the step should be sufficiently large to make the system react quickly to accommodate rapid environmental changes. On the other hand, the step should be as small as possible, avoiding unnecessary large oscillations during steady-state operations. Introducing a varying step size is one way of addressing this trade-off. However, variable step size P&O-algorithms may have a weakness toward rapid environmental changes [31, 32, 35]. They usually base the following step size and direction entirely on the observed change, and therefore cannot distinguish whether the change has occurred due to the shifting point of

operation or due to environmental changes. As a result, the algorithm may introduce a significant step away from the new maximum power point, rather than toward it.

In this project, P&O-algorithms will be investigated and used as optimization procedures. By introducing a P&O-algorithm, the novel coalescing pump will be guided toward the optimal point of operation in small steps by comparing current and previous process measurements. If the optimal point of operation changes, e.g., due to varying upstream conditions, the algorithm will automatically guide the pump toward the new optimum, ensuring optimal droplet growth and downstream separation efficiency.

1.5 Main hypothesis

The main hypothesis behind the work of this thesis is that real-time process information can be used in active control of the novel coalescing pump to maximize the efficiency of downstream produced water treatment equipment.

1.6 Objectives

The hypothesis will be verified through the following four objectives:

Objective 1: Study the coalescing performance of the novel pump.

Objective 2: Study the characteristics of the pump-hydrocyclone combination.

Objective 3: Implement and study the considered control strategies.

Objective 4: Improve the control strategy recommended by Objective 3.

1.7 Appended papers

Paper A investigates the coalescing effect of the novel multistage centrifugal pump with respect to the point of operation and water characteristics. Laboratory testing is performed with synthetic produced-water containing stabilized crude oil. The coalescing effect is studied by comparing the droplet size distribution at the inlet and outlet of the pump using online measurements. The study is performed for different combinations of inlet droplet size distribution, oil concentration, oil type, flow rate and pumping pressure.

Paper B studies the benefits of combining the coalescing pump with a deoiling hydrocyclone. The study shows how the coalescing centrifugal pump increases the separation

efficiency. Furthermore, it is shown that the pumping pressure can be adjusted to maximize the improvement. Experimental results demonstrate how pumping conditions that minimize the volume fraction of droplets smaller than the hydrocyclone cut size, maximize the separation efficiency. It is also demonstrated how the concept of continuous pumping-pressure optimization can be implemented in a low-pressure produced water treatment plant.

Paper C presents the development and implementation of the considered control strategies. A P&O-algorithm is developed and implemented in two of the strategies, one with the oil-in-water analyzer in the *midstream* position, and the other with the analyzer in the *downstream* position. The latter is recommended and considered most robust, as it requires no prior knowledge of the system. The two setups are also compared to a third setup, in which the optimal point of operation is predicted based on measurements having the analyzer in the *upstream* position.

Paper D presents further developments of the control strategy having the oil-in-water analyzer in the *downstream* position. Three alternative variable step size P&O-algorithms are developed to tackle general drawbacks. Due to the variable step size, the controllers react rapidly to changes in the upstream produced water characteristics, at the same time as they reduce (or eliminate) steady-state oscillations. Based on both simulation and experimental testing, the study discusses the advantages and disadvantages of each algorithm, respectively.

1.8 Thesis outline

This thesis is divided into six chapters: Chapter 1 introduces the project background and motivation, in addition to the objectives, the thesis structure, and the appended papers. Chapter 2 introduces the origin, characteristics, monitoring, and management of produced water, in addition to national and international regulations relating to the handling of produced water. Chapter 3 discusses phenomena related to oil droplet formation and removal, Chapter 4 presents the experimental methodology, Chapter 5 summarizes the experimental work and discusses the main findings, and Chapter 6 presents the project conclusions and discusses further work.

Chapter 2

Produced water

This chapter introduces the origin, characteristics, monitoring, and management of produced water, and presents national and international regulations relating to the handling of produced water in the North Sea and on the Norwegian continental shelf.

2.1 Origin

For a new well, water is usually absent or makes up just a small percentage of the produced fluids, increasing as the production continues and the well matures [11]. Connate water is initially trapped in the underground formations structures where it co-exists with hydrocarbons in overlapping layers due to differences in density [11]. As hydrocarbons are removed from the formation, the internal pressure gradients change, making the water rise toward the well [11].

Water is sometimes injected (and produced water re-injected) into the reservoir to maintain the hydraulic pressure and to enhance the oil recovery. Shortly after injection, the water may find its way to the production zone, increasing the amount of water being produced [5, 11]. Loss of mechanical integrity of the reservoir structure can lead to water breaking through the production zone, also increasing the water cut [5, 11].

2.2 Characteristics

The characteristics of produced water vary between fields and even between wells in the same field. Several factors can affect the volume and characteristics of the produced water during the lifetime of the well, e.g., the type of well drilled and its location within the reservoir structure [5, 11]. Factors such as the geological location of the field, the field's geological formation and characteristics, the lifetime of the reservoirs, and the type of hydrocarbon products being produced are other factors affecting the volume and

properties of the produced water [5, 11]. Water injection may make these properties vary even more dramatically [11].

Produced water contains both organic and inorganic compounds; many of them are toxic [5]. Some of the compounds are naturally occurring in the produced water, while others are related to chemicals added for reservoir stimulation and well-control purposes [5, 11]. Describing produced water with a single set of chemical properties and concentrations is not a straightforward process. However, the following categories and components are generally found [13]:

- Oil and organic chemical compounds such as benzene, toluene, ethylbenzene and xylene (BTEX), and polycyclic aromatic hydrocarbon (PAH).
- Various naturally occurring inorganic substances and particles (e.g., calcium, magnesium, sulfate, and barium).
- Chemical additives used for drilling, reservoir stimulation, and well operation (e.g., biocides and corrosion inhibitors).
- Naturally-occurring radioactive materials (NORMs).

2.3 Regulations

In the North Sea, both international recommendations and national regulations govern the discharge of produced water. OSPAR, the Oslo - Paris Commission, is a mechanism by which Norway cooperate with the European Union (EU) and 14 other governments to protect the marine environment of the North-East Atlantic [36]. OSPAR Recommendation 2001/1 focuses on oil in produced water and the application of best available technique (BAT) and best environmental practice (BEP). According to the recommendation,

> Contracting Parties should ensure that BAT and BEP are applied on each installation and that BAT and BEP are regularly reviewed...
>
> No individual offshore installation should exceed a performance standard for dispersed oil of 30 mg/l for produced water discharged into the sea. [10]

The Petroleum Safety Authority establishes pollution control parameters for the petroleum industry and supervises activities in this sector [37]. The Activities Regulations Chapter XI, Section 60, includes, amongst others, the following regulations:

> Produced water shall be cleaned prior to discharge to sea.
>
> The oil content in produced water discharged to sea, shall be as low as possible... In any event, the oil content shall not exceed 30 mg oil per litre of water as a weighted average for one calendar month.

> On facilities that discharge produced water, the operator shall perform environmental risk assessments of the discharges. These shall be performed as soon as possible after produced water is available. New risk assessments shall be performed in case of significant changes in the discharge or in any event minimum every five years...
>
> Water treatment systems shall be designed and operated such that the environmental strain from discharges to sea will be as low as possible also if the discharge limitations, ..., can be met with reduced treatment effect. The operator shall establish and maintain a best practice for operating and maintaining the processing system, comprising treatment units incorporated in the system on the individual facility.
>
> The operator shall regularly assess possible technical solutions that can reduce the environmental strain from discharges of oily water... [38]

Discharges of produced water also contain substances other than oil, initially present in the reservoir or added chemicals. Therefore, in 2012, OSPAR introduced *a risk-based approach to the Management of Produced Water Discharges from Offshore Installations*. The risk-based approach is a method of prioritizing those discharges and substances that pose the highest risk to the environment [39].

In addition to the OSPAR limits, the Norwegian government issued White Paper No. 58 [40], requiring the oil industry to develop strategies to reach zero harmful environmental discharges of produced water [41]. The zero-discharge goal comprises both releases of oil and naturally occurring substances, including radioactive materials and added chemicals [16].

To assist in achieving the zero-discharge goal, an indicator for the potential impact of produced water releases was developed and named the environmental impact factor (EIF) [42]. The EIF is based on a combined environmental risk and hazard assessment, accounting for both the composition and the amount of the discharge [41].

2.4 Monitoring

The measured amount of oil in produced water is a method-dependent parameter, and reference methods are therefore necessary to compare results [43]. OSPAR makes a distinction between total oil and dispersed oil, where dispersed oil content is determined based on the reference method described in Agreement 2005-15 [44], and total oil means the total amount of hydrocarbons, including both dispersed and dissolved oil [43]. Dispersed oil usually refers to oil in the form of small droplets, containing both aliphatic and

aromatic hydrocarbons, while dissolved oil usually means oil in a soluble form, mostly consisting of aromatic hydrocarbons and organic acids [43].

Reference methods are not always user-friendly or practical and, therefore, alternative methods have been developed. Bench-top instruments are often used for routine analysis, and the results can be correlated to reference methods [43]. Online monitors are used for process trending and to detect deviations. Such monitors are advantageous with regards to process control, management and optimization, as they provide information about the produced water continuously [43].

The environmental risk from discharges of produced water depends not only on the concentration of dispersed oil but also on dissolved oil and other components such as production chemicals [13]. To assess the risk that produced water may cause to the environment, the following methods can be used [5]:

- Testing substances on animals or another biota.
- Scientifically monitoring of the discharge.
- Theoretical modeling.

2.5 Management

The purpose of OSPAR Recommendation 2001/1 is "to prevent and eliminate pollution by oil and other substances caused by discharges of produced water into the sea" [10]. Here, *other substances* is defined as all or any of the following:

- Solid particles from the reservoir;
- substances from the reservoir such as heavy metals;
- particles of scale and corrosion products;
- residues of chemicals injected at various points in the production system, for purposes such as controlling scaling, corrosion, foaming, bacterial growth or emulsion; and
- chemicals used in drilling and completing wells which are reintroduced into the production system during clean-up operations. [10]

Hence, the primary goal of produced water treatment is oil removal and the removal of other environmentally harmful components. Four primary steps can be identified to minimize the production and environmental impact of produced water [13]:

1. Avoid producing water.

Water reduction is primarily performed using so-called water shut-off techniques, involving the use of chemical methods to physically prevent reservoir water from reaching the well [45, 46]. One of the most common methods for water shut-off is injecting various chemicals and components such as silica, wax, and different types of gel. Also, mechanical measures for drilling and cementing can be used to affect the structure and permeability of various zones in the reservoir [13, 46].

Downhole separation removes the produced water from oil and gas at the bottom of the well, re-injecting most of the water. The oil and gas enriched streams are routed toward the surface for further treatment [45, 46]. A subsea separation system separates the fluids on the seabed before sending the produced oil and gas to the surface for further treatment. The separated water may be re-injected back into the formation for disposal or pressure maintenance [11, 45].

2. Treat the water before discharge.

Due to the vast quantities of offshore produced water brought to the surface, transportation to land is normally not realistic. The water must, therefore, be sufficiently treated on the installation before being discharged or re-injected [13]. Lack of space encourages the use of compact methods, either chemical or physical based [47]. Offshore produced water is conventionally treated through gravity-based separation systems [48]. Among many different technologies available, the selection of treatment methods varies according to factors such as chemical and physical properties of the water, the flow rate, end-use, regulations, and technical and economic feasibility [48].

OSPAR issued in 2013 the *Background Document concerning Techniques for the Management of Produced Water from Offshore Installations*, where an overview of various techniques for the removal of heavy metals, dissolved oil, dispersed oil and offshore chemicals from the produced water are presented [46]. The intention is to revise this document regularly to update the data as experience increases, and to allow for the inclusion for new techniques. The OSPAR background document emphasizes that the success of any method is dependent, among other factors, on the local environment, e.g., the local reservoir conditions and the local operational conditions [46]. It cannot be concluded that a method, which has been operated successfully at one installation, will achieve the same results at another location [46].

In the North Sea, a typical treatment system consists of three-phase separation, with hydrocyclones on the water discharge [17]. The water treated in the hydrocyclone is typically routed to a degassing vessel, and the final stage of the water treatment is often a

compact flotation unit [17]. Flotation flocculant may be added upstream of the degassing vessel [17]. The oil recovered from the water treatment process is usually fed back to the oil treatment facility [49], and the amount of water in the recovered mixture should, therefore, be as low as possible. In 2015, it was found that all facilities on the Norwegian continental shelf discharging offshore water to the sea, had installed hydrocyclones, centrifuges or flotation cells to meet the regulatory requirements for discharges of dispersed oil. Also, to meet the zero-emission targets, additional cleaning methods had been installed in many fields [15].

3. Reduce the amount of water discharged to the environment.

On the Norwegian continental shelf, the main strategies for handling treated produced water are injection or discharge [15]. Produced water injection or re-injection is carried out for two reasons, where one reason is to support the reservoir pressure. Injection for pressure support is called re-injection, meaning that the produced water is returned to its original reservoir or another producing reservoir. The other reason for water injection is disposal. Produced water may, in this case, be injected into a geological formation that is not in contact with the producing reservoir, reducing the amount of water being discharged to the environment [13].

For some fields, injection or re-injection is considered BAT [46], while for others, it may not be feasible due to geological or technical reasons. The treatment requirements for re-injected produced water are location-specific, but 5 % discharges to sea must be taken into account due to planned and unplanned shutdowns [13]. Therefore, fields often have full treatment of water that is being (re-)injected, while other fields may have large buffer tanks to avoid discharge to the sea during periods of injection downtime [13, 15].

4. Prevent the impact of emissions.

Preventing the negative impact of discharges can be done by minimizing the use of production chemicals or selecting non-harmful chemicals [13]. Increasing the treatment efficiency by optimizing the processes and systems handling the water will also reduce the impact [13]. By modeling the emissions and calculating EIF in the design phase, production chemicals can be selected to reduce the environmental load [13]. Through continuous monitoring of the treatment plant and other processes related to the produced water, activities and measures increasing the efficiency and performance of the handling can be identified [13].

Chapter 3

Oil droplet formation and removal

This chapter discusses oil droplet formation and the relationship between the droplet size and the efficiency of typical produced water treatment technologies, focusing particularly on deoiling hydrocyclones.

3.1 Droplet formation

Tight oil/water emulsions may be formed in turbulent flow; in general, the higher the turbulence intensity, the smaller the droplets of oil or water [6]. In a production facility, there are many highly turbulent flow regions and regions where droplets are subjected to shear stress [6]. First, fluids experience shear stress in the reservoir, near the wellbore. Later, lifting techniques such as electrical submersible pumps may introduce high-intensity turbulence, as may also the wellhead choke [6]. As the fluids travel throughout the production facility, control valves and pumps may be additional sources of shear stress and droplet breakage [6, 7].

Focusing on oil droplets dispersed in water, which is most relevant for produced water systems, a phenomenon counteracting the droplet breakup is droplet-droplet coalescence. To what extent one of these phenomena is dominating, is affected by both produced water characteristics and the hydrodynamics. Produced water characteristics involve factors such as the oil concentration, droplet size distribution, oil and water density, oil and water viscosity, water temperature and salinity, and surfactants [50, 51, 52, 53]. All these factors affect the interfacial interactions between the two phases. In addition, the amount of time the droplets are exposed to the turbulent environment, influences the resulting droplet size distribution.

3.1.1 Droplet size distribution

Figure 3.1 illustrates a typical volume-based droplet size distribution. In the figure, the x-axis shows the droplet diameter, d, logarithmically. The right y-axis, H, is the fraction of the total volume constituted by droplets of diameter d, while the left y-axis, F_{H}, is the cumulative volume of droplets smaller than, or equal, to d. The volume median droplet diameter, d_{v50}, is also indicated in the figure. This is the size which 50 % of the total volume of droplets are either smaller than or equal to [54].

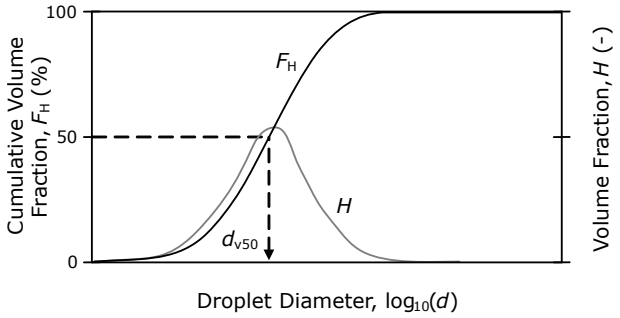

Figure 3.1: Illustration of a typical volume-based droplet size distribution.

The size of the droplets and the shape of the distribution may change due to droplet breakup, droplet-droplet coalescence or separation processes [17]. Distributions such as the one in the illustration, are often modeled using either log-normal or Rosin-Rammler distribution functions [17]. Bi-modal distributions are also observed; these distributions have two distinct peaks rather than one, and are typically observed where high shear stress occurs [17].

3.1.2 Turbulence intensity

The size of the oil droplets is highly influenced by collisions with flow eddies of roughly the same size [6]. The kinetic energy of these eddies depends on the turbulent energy dissipation rate per unit mass, ε, which is a measure of the turbulence intensity [6]. The following are discussions of the turbulent energy dissipation rate in pipes, valves, and pumps.

Energy dissipation in pipes

According to the so-called Darcy-Weisbach equation, the energy dissipation per unit mass, h, in turbulent pipe flow can be expressed as [6, 55]:

$$h = \frac{1}{2} \cdot \frac{f \cdot L}{D} \cdot u^2, \tag{3.1}$$

where f is a friction factor, L is the length of the pipe segment, D is the pipe diameter and u is the mean flow velocity.

If the pipe segment is chosen so that the flow is relatively similar with regards to flow rate, Q, area, A, and turbulence, the rate of energy dissipation is given by h/t [6]. Here, t is the time required for the fluid to travel through the pipe, given by $t = L/u$, where $u = Q/A$. The energy dissipation rate is then given by [6]:

$$\varepsilon = \frac{h}{t} = \frac{1}{2} \cdot \frac{f}{D} \cdot u^3. \tag{3.2}$$

From Eq. 3.2, it is seen that low energy dissipation rate can be achieved by choosing pipes and bends with a large diameter and a low friction factor. Generally, the turbulence intensity in pipes and flowlines is relatively low [6]. Droplet-droplet coalescence and droplet growth are therefore often found in pipe flow, increasing the average droplet size.

Energy dissipation in valves

Assuming parts of the turbulent energy are immediately transferred to heat in a dissipation volume, V, the energy dissipation rate per unit mass through a valve can be expressed as [19, 52]:

$$\varepsilon = \frac{\Delta p_{\mathrm{v}} \cdot Q}{\rho_{\mathrm{c}} \cdot V}, \tag{3.3}$$

where Δp_{v} is the permanent pressure drop and ρ_{c} is the continuous phase density.

Valves with increased dissipation volume, V, have been designed to reduce the energy dissipation rate [19, 56]. Such valves are examples of so-called *low shear* valves, introducing reduced shear stresses. Having two valves in series has also been found to reduce the droplet breakage, as the pressure drop across each valve, Δp_{v}, is reduced [52].

Energy dissipation in pumps

Recalling the ranking of pumps with regards to how they affect the droplet size (Section 1.3.2), it is evident that droplet breakup in pumps highly depends on the pump type, design, and operation.

By assuming the turbulent energy dissipation rate per unit mass in conventional centrifugal pumps is proportional to the hydraulic energy provided by the pump per unit mass, methods have been proposed to predict the most likely downstream droplet size distribution, focusing on droplet breakup [57, 58]. As the novel multistage centrifugal pump, which is considered in the work of this thesis, promotes a combination of droplet breakup and droplet-droplet coalescence, also coalescence mechanisms are necessary to estimate the effluent droplet size distribution.

3.1.3 Droplet breakup

The mechanism of droplet breakup is typically expressed as a balance between the external stresses from the continuous phase and the surface stress of the droplet, plus the viscous stress of the fluid inside the droplet [6, 51]. The external stresses may destroy the droplet, while the surface stress and viscous stress restore the droplet's form. The balance of these stresses leads to a maximum stable droplet diameter, $d_{\max}$. For droplets larger than $d_{\max}$, the restorative stress will be overcome by the external stress, and the droplet breaks [6, 51].

Models developed by Hinze [59] are often the basis to gain an understanding of droplet breakup [50, 60]. These models apply the concept of a cascade of turbulent eddies, introduced by Kolmogorov, which assumes homogeneous isotropic turbulence [60]. Eq. 3.4 shows a version of the model, focusing on droplets larger than the Kolmogorov length scale in dilute liquid-liquid systems with a low viscosity dispersed phase [50, 60]:

$$d_{\max} \propto \left(\frac{\sigma}{\rho_{\mathrm{c}}}\right)^{3/5} \cdot \varepsilon^{-2/5}, \tag{3.4}$$

where σ is the interfacial tension.

As seen from Eq. 3.4, the size of the largest droplets is influenced by the turbulence intensity, the continuous phase density, and the interfacial tension. Low interfacial tension can result in small droplets; in produced water, low interfacial tension may be the result of naturally occurring polar molecules or excessive use of production chemicals [6].

3.1.4 Droplet-droplet coalescence

The most common model for droplet-droplet coalescence is the film drainage model [53]. According to this model, the coalescence process in turbulent flow is divided into (1) collision of droplets, and (2) drainage of the fluid film between them [52, 53]. The fluid film is formed by water trapped between the droplets. Figure 3.2 shows an illustration of the coalescence process where two droplets collide and coalesce.

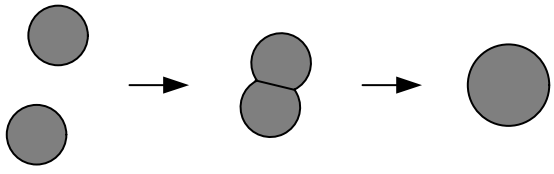

Figure 3.2: Illustrated droplet-droplet coalescence process.

Among other parameters, the coalescence rate is governed by the intensity of the turbulence, the number and size of the droplets, and fluid properties such as viscosity, density, and interfacial tension [52, 53]. The collision frequency, i.e., how often two droplets collide,

increases as the number of droplets, the size of the droplets, or the turbulence intensity is increased [52, 53]. Whether a collision leads to coalescence is determined by the coalescence probability. This probability is governed by the time it takes to drain the fluid film and the droplet-droplet interaction time [52, 53], where increased turbulence intensity may reduce the latter. The amount of time turbulence is present is also an essential factor for the total number of collisions.

3.2 Oil removal efficiency

Primary and secondary topside water treatment usually consists of a combination of gravitation, enhanced gravitation, and flotation techniques [12]. For such technologies, the mechanism for oil removal is primarily based on droplet buoyancy, and can, therefore, be described using Stokes' law [12].

3.2.1 Gravity separation

The unhindered laminar terminal velocity, v_t, of a spherical oil droplet in water is estimated based on the gravitational acceleration, g, the droplet's diameter, d, and mass density of the oil, ρ_o, the mass density of the surrounding water, ρ_w, and the dynamic viscosity of the water, μ_w. The force balance ($F_d = F_g$) between Stokes' drag force (Eq. 3.5), and the excess force due to the difference between the weight and buoyancy of the droplet (Eq. 3.6), yields the terminal settling velocity (Eq. 3.7) [19, 61]:

$$F_d = 3 \cdot \pi \cdot \mu_w \cdot v_t \cdot d, \tag{3.5}$$

$$F_g = \frac{\pi \cdot (\rho_w - \rho_o) \cdot g \cdot d^3}{6}, \tag{3.6}$$

$$v_t = \frac{(\rho_w - \rho_o) \cdot g \cdot d^2}{18 \cdot \mu_w}. \tag{3.7}$$

Examining Eq. 3.7, it is observed that the terminal settling velocity, and subsequently the oil removal efficiency of gravitational technologies, highly depends on the droplet size. Also, although to a lesser extent, the efficiency depends on the oil/water characteristics and the temperature of the mixture, where the latter affects μ_w, ρ_o and ρ_w [12].

To separate fluids with different density, gravity separation is used in, e.g., three-phase separators and gas flotation units. For the separation of water in a three-phase separator, the goal is for the oil droplets to rise so that cleaned water can be extracted from the bottom of the vessel [62]. A flotation unit works similarly; however, the oil droplets here

attach to gas bubbles, reducing the density and increasing the size, and thus increasing the terminal velocity [14, 46].

Another way of increasing the terminal velocity is by increasing the gravitational force; this is called *enhanced gravity separation*. Hydrocyclones and centrifuges are enhanced gravity separators, where radial acceleration speeds up the terminal velocity [46, 63].

3.2.2 Hydrocyclone separation

Figure 3.3 illustrates a hydrocyclone, including a sketch of the internal flow structure. The produced water enters the hydrocyclone through one or more tangential inlets, developing a vortex system. In the vortex system, the lighter phase (oil) migrates toward the center axis as the heavier phase (water) is forced toward the cylinder wall [18, 19]. The cleaned water exits through the so-called underflow outlet, while the oil-enriched water exits through the overflow outlet.

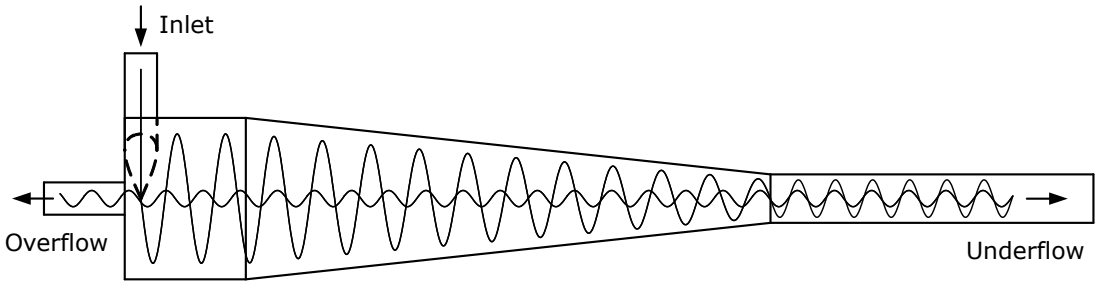

Figure 3.3: Sketched hydrocyclone with the internal flow structure.

In addition to factors such as design and fluid properties, the hydrocyclone performance depends on the flow rate and the flow split [19]. Both too low and too high flow rate results in reduced separation efficiency, and the flow rate should, therefore, be kept within an efficiency plateau defined by a minimum and a maximum flow rate [8, 20]. Low flow rates can cause the vortex system to not fully develop, whereas high flow rates may result in high turbulence and lack of pressure gradients driving the oil-core through the overflow [8, 20]. The flow split is the ratio between the overflow and underflow flow rate, and is approximately proportional to the PDR between the two outlet pressures relative to the inlet pressure [23]. The hydrocyclone separation efficiency increases as the flow split is increased, until it levels off and becomes essentially constant [8, 20]. It is desirable to have as high oil concentration as possible in the overflow, reducing the volume of rejected water [19, 20]. The flow split should, therefore, be kept constant and as low as possible, without compromising on the separation efficiency.

Fluids rotating in the hydrocyclone are exposed to radial acceleration, a_{r}, which can

be expressed as [19]:

$$a_{\mathrm{r}} = \frac{{v_{\mathrm{T}}}^2}{r}, \tag{3.8}$$

where v_{T} is the tangential velocity and r is the distance from the cyclone center core. Assuming the fluid surrounding the droplets possesses laminar behavior, Eq. 3.7 can be modified to include the magnified acceleration [19, 64]:

$$v_{\mathrm{t}} = \frac{(\rho_{\mathrm{w}} - \rho_{\mathrm{o}}) \cdot {v_{\mathrm{T}}}^2 \cdot d^2}{18 \cdot \mu_{\mathrm{w}} \cdot r}. \tag{3.9}$$

Eq. 3.9 is a simplified model of the droplet migration in a deoiling hydrocyclone; however, it clearly illustrates the importance of large oil droplets for high separation efficiency.

Quantitatively, the hydrocyclone separation efficiency, E_{HC}, may be defined as [19, 65]:

$$E_{\mathrm{HC}} = \left(1 - \frac{C_{\mathrm{uf}}}{C_{\mathrm{in}}}\right) \cdot 100\ \%, \tag{3.10}$$

where C_{in} is the inlet oil concentration, and C_{uf} is the underflow oil concentration. Qualitatively, the separation performance can be presented as a separation probability curve, called the migration probability curve. This curve is defined as the probability, G, that a droplet of diameter d leaves the hydrocyclone through the overflow outlet [19, 65]. Figure 3.4 illustrates a typical migration probability curve for deoiling hydrocyclones. The illustration highlights the cut-size, d_{50}, which is the diameter of a droplet with 50 % migration probability [19, 65].

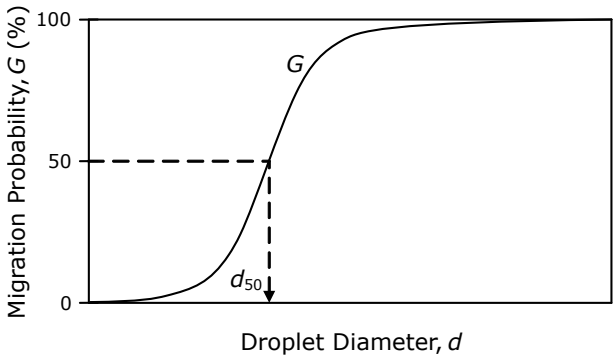

Figure 3.4: Illustration of a typical migration probability curve.

For commercial hydrocyclones, the migration probability curve is often provided by the supplier. Alternatively, the curve may be estimated experimentally by measuring the inlet and outlet droplet size distribution, in combination with oil concentration measurements, using Eq. 3.11 [65],

$$G(d) = \left(1 - \frac{C_{\mathrm{uf}} \cdot H_{\mathrm{uf}}(d)}{C_{\mathrm{in}} \cdot H_{\mathrm{in}}(d)}\right) \cdot 100\ \%, \tag{3.11}$$

where H_{in} and H_{uf} are the inlet and underflow droplet size distribution, respectively. Knowing both the migration probability curve and the inlet droplet size distribution, Eq. 3.12 can be used to predict the hydrocyclone separation efficiency [65],

$$E_{\text{HC}} = \sum_{d=0}^{\infty} \left(H_{\text{in}}(d) \cdot G(d) \right). \tag{3.12}$$

3.2.3 Simplified hydrocyclone efficiency estimation

Through the work of this project, a simplified method of predicting the resulting separation efficiency has been suggested [3]. Here, the separation efficiency is assumed to be a step-function, stepping from 0 to 100 % at $d = d_{\text{lim}}$, where d_{lim} is a limit size. The gray dotted line in the right plot of Figure 3.5 illustrates this step-function.

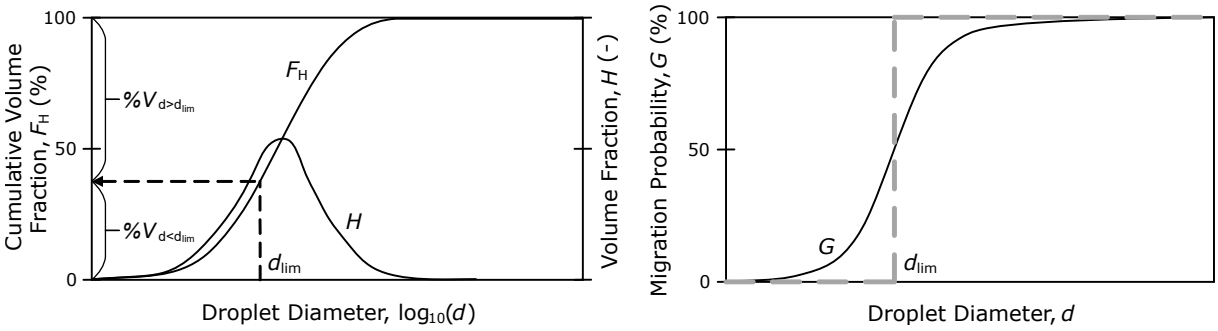

Figure 3.5: Illustration of d_{lim} and $\%V_{\text{d>d}_{\text{lim}}}$.

By assuming the migration probability is 100 % for $d > d_{\text{lim}}$, the hydrocyclone separation efficiency may be predicted as follows [3]:

$$E_{HC} = \sum_{d=d_{\text{lim}}}^{\infty} H_{\text{in}}(d) \cdot 100\ \% = \%V_{\text{d>d}_{\text{lim}}}, \tag{3.13}$$

where $\%V_{\text{d>d}_{\text{lim}}}$ is the volume fraction of droplets larger than d_{lim}, illustrated in the left plot of Figure 3.5.

Chapter 4

Experimental methodology

A test rig, located at Typhonix Test Center in Norway and shown in Figure 4.1, was designed and built in the initial phase of this project. This chapter describes the rig and equipment used in the experimental work.

Figure 4.1: Picture of the test rig.

4.1 Functional description

Figure 4.2 is a schematic representation of the test rig. The rig was a *once-through* system, meaning the test fluids were collected in a disposal tank rather than being reused. From left to right, the rig consisted of a *feeding pump*, an *oil-injection pump*, a *mixing valve*, the *coalescing pump*, a *hydrocyclone*, and two control valves (CVs), referred to as *CVo* and

CVd, respectively. An online oil-in-water analyzer was arranged and shifted from one to the other of the isokinetic sampling points indicated in the schematics. The main stream flowed through the rig in 1 in. stainless steel tubing, while the tubing for oil injection and sampling were 1/4 in. and the hydrocyclone overflow section was 1/2 in. tubing. Ball valves were used to isolate the equipment and sampling points not used during a specific test.

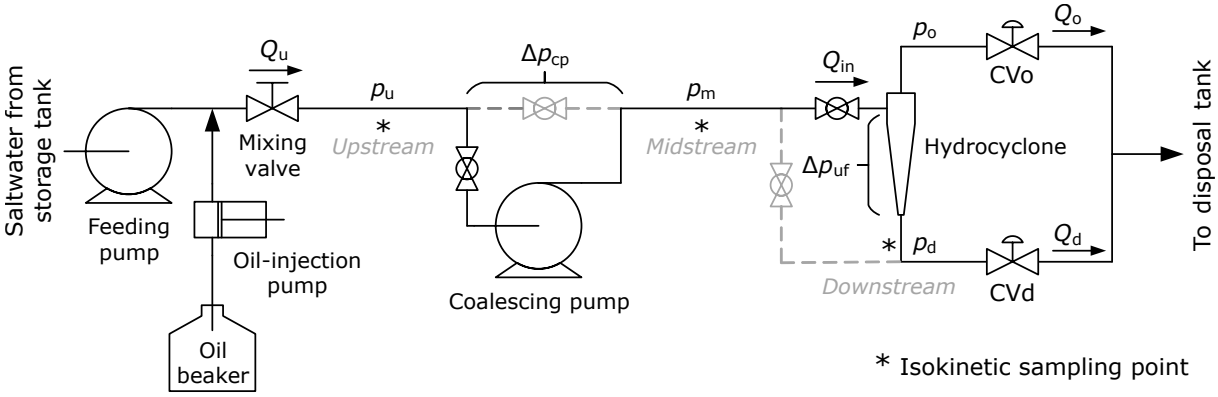

Figure 4.2: Test rig schematics.

The feeding pump transported heated saltwater from a storage tank to the test rig, keeping the flow rate, Q_u, constant. The oil-injection pump continuously injected oil into the saltwater stream, creating synthetic produced-water with a known oil concentration, C_u. The manually operated mixing valve ensured proper oil/water mixing, and the opening of the mixing valve, and consequently the pressure drop, was adjusted to the position resulting in the desired volume median droplet diameter, $d_{v50,u}$, upstream of the coalescing pump. The synthetic produced-water was thereafter fed to the hydrocyclone, either through or bypassing the coalescing pump. After being separated in the hydrocyclone, the cleaned water exited through the hydrocyclone underflow outlet, flowing toward CVd. This control valve was used to control the pressure upstream of the coalescing pump, p_u. The oil-enriched water leaving the hydrocyclone through the overflow outlet, flowed toward CVo. This valve was used to control the hydrocyclone PDR. Downstream of the hydrocyclone, the fluid streams were joined together and collected in a disposal tank. Alternatively, the hydrocyclone could be bypassed, leading the fluid stream directly through CVd and toward the disposal tank.

4.2 Equipment

Figure 4.3 shows a close-up photo of the test rig, identifying the feeding pump (1), the oil-injection pump (2), the mixing valve (3), the coalescing pump (4), the oil-in-water analyzer (5), the hydrocyclone (6), CVd and CVo (7), and a vertical batch-separator (8).

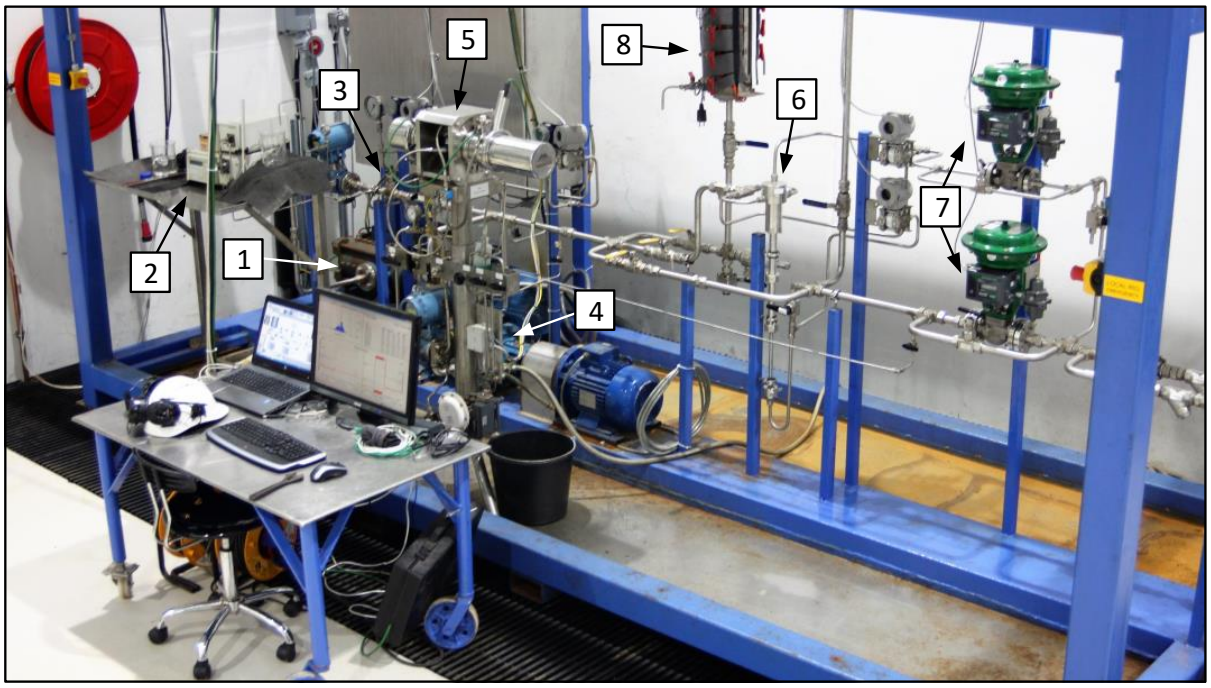

Figure 4.3: Close-up photo of the test rig with the main components identified.

4.2.1 Feeding pump

The feeding pump was a conventional horizontal multistage centrifugal pump, driven by an asynchronous alternating current (AC) motor using a VFD. The rotational speed of the pump/motor assembly was controlled according to the desired flow rate, Q_{u}, by a closed-loop PI-controller.

4.2.2 Oil-injection pump

A Gilson 305 piston pump was used to inject the desired amount of oil into the saltwater stream. The oil entered the center of the pipe, upstream of the mixing valve, through a tube bent in the same direction as the saltwater flow. Figure 4.4 shows a picture and schematics of the oil-injection pump assembly.

During injection, the oil was stored in a beaker and stirred using a magnetic mixer. The piston module with a maximum flow rate closest to, and higher than, the desired flow rate was chosen to maximize the pumping frequency, reducing the amplitude and increasing the frequency of the ripples. In addition, the oil went through an accumulator module which further reduced the ripples and secured a steady flow. The manufacturer specifies a maximum accuracy error of ± 1 % for water over the full flow rate and pressure ranges. However, as the pumped fluids were oils, which have higher viscosity compared to water and may contain particles, the flow rate was manually verified.

A three-way valve was installed, enabling the oil to be re-circled when not injected

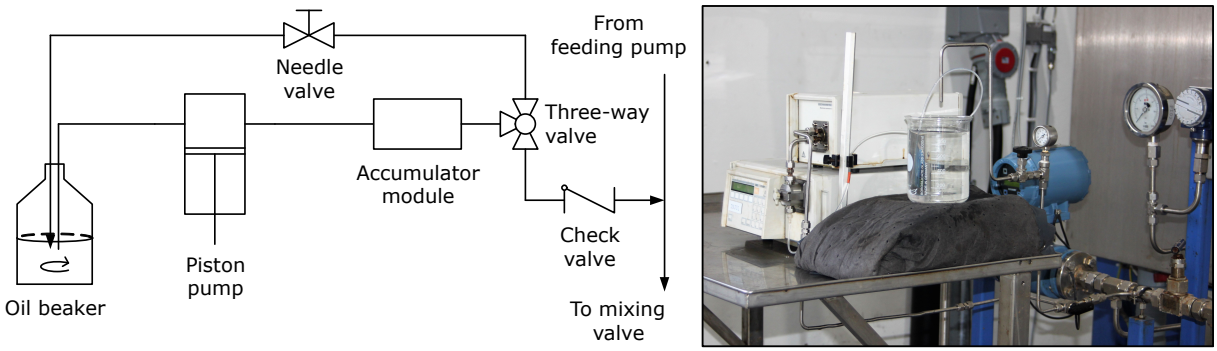

Figure 4.4: Left: Schematics of the oil-injection pump assembly. Right: Picture of the oil-injection pump assembly.

into the saltwater stream. The re-circle line included a needle valve to pressurize the accumulator module, and was used during flow rate inspection. A check valve secured the saltwater from flowing into the oil-injection assembly.

4.2.3 Mixing valve

An 1 in. manually operated Swagelok SS-12NBS16 Severe-Service Union-Bonnet Needle Valve was used to mix the injected oil into the saltwater stream. Figure 4.5 shows a picture of the mixing valve. In the picture, the oil-injection tube and the three-way valve are seen in the lower left corner.

Figure 4.5: Picture of the oil/water mixing valve.

4.2.4 Coalescing pump

The coalescing pump, introduced in Section 1.3.3, was a seven-stage horizontal multi-stage centrifugal pump designed according to the principles of Typhonix AS [66]. Note that the pump was a small-scale version of the commercially available pumps, but the

overall trends observed are assumed to be the same for any coalescing centrifugal pump design and size [1]. Figure 4.6 shows a picture of the coalescing pump, which was driven by an asynchronous AC motor, using a VFD. The rotational speed of the pump/motor assembly was controlled according to the desired pumping pressure, Δp_{cp}, defined as $\Delta p_{\mathrm{cp}} = p_{\mathrm{m}} - p_{\mathrm{u}}$, by a closed-loop PI-controller.

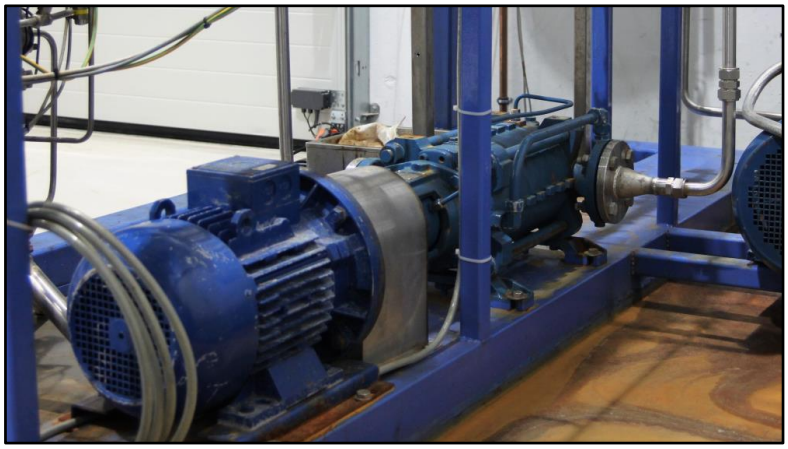

Figure 4.6: Picture of the coalescing multistage centrifugal pump.

4.2.5 Oil-in-water analyzers

A Malvern Insitec was used as the online oil-in-water analyzer, continuously measuring droplet size distribution and oil concentration trends. In addition, a Turner Design (TD) 500D was used to measure the real oil concentration, verifying measurements of the Malvern Insitec during crude oil testing.

Figure 4.7 shows pictures of the oil-in-water analyzers. In the figure, the left picture shows the Insitec installed on a custom-made flow-control assembly. The upper right picture shows bottle sampling for the TD 500D oil-in-water analysis shown in the lower right picture.

The Malvern Insitec is a laser-diffraction analyzer, measuring the light-scattering pattern in a flow-cell and employing *Mie Theory* to determine the size of the oil droplets [54]. The analyzer was equipped with a 200 mm focal lens, calibrated and certified by the supplier. During crude oil testing, a standard refractive index of $1.5 + 0.001\mathrm{i}$ was used. When Exxsol was used, the refractive index was $1.44 + 0.001\mathrm{i}$. For water (the continuous phase), the refractive index was $1.33 + 0\mathrm{i}$.

The flow-control assembly contained a flow meter and a control valve which were used to control the sampling flow rate, Q_{s}. The assembly also allowed for periodically flushing and cleaning the flow-cell during testing. Continuous isokinetic sampling was achieved using sampling tubes like the one shown in Figure 4.8. In the schematics, u_{s} is the flow

Figure 4.7: Left: Picture of the Insitec installed on a custom-made flow-control assembly. Upper right: Picture of bottle sampling. Lower right: Picture of TD 500D oil-in-water analysis.

velocity of the fluid sample and u_{PW} is the produced-water flow velocity; these velocities must be equal during isokinetic sampling [43].

Figure 4.8: Left: Schematics of the isokinetic sampling tubes. Right: Picture of an isokinetic sampling tube.

The TD 500D is a hand-held fluorometer used to measure the concentration of oil in produced-water samples obtained during crude oil testing [67]. The measurements were conducted directly on the produced-water sample, and prepared solutions containing

10 ppm to 1000 ppm oil in water were used to calibrate the instrument.

4.2.6 Hydrocyclone

The hydrocyclone used in this project was a non-commercial liner built and used by [19] in the study of operational control of deoiling hydrocyclones. In Figure 4.9, the left picture shows the hydrocyclone mounted in the test rig. The right picture shows CVo and CVd, in addition to a sampling point used to measure the overflow flow rate, Q_o.

Figure 4.9: Left: Photo of the hydrocyclone mounted in the test rig. Right: Picture of CVo, CVd and a sampling point.

In the hydrocyclone, the synthetic produced-water entered a cylindrical inlet section with diameter 40 mm through two tangential inlets, each having a diameter of 6 mm. Following the cylindrical inlet section, there were a cone of 1.5° and a cone of 15°. Next, a cylindrical section of length 235 mm and diameter 10 mm followed the two cones. The diameter of the overflow orifice was 1 mm, and the total internal volume was 0.20 liter. Detailed technical drawings of the hydrocyclone liner can be found in [19].

During testing, the hydrocyclone PDR, φ_{PDR}, was kept constant using CVo, and was defined as:

$$\varphi_{\mathrm{PDR}} = \frac{p_{\mathrm{m}} - p_{\mathrm{o}}}{p_{\mathrm{m}} - p_{\mathrm{d}}}, \tag{4.1}$$

where p_m is the pressure at the hydrocyclone inlet, p_o is the overflow pressure and p_d is the underflow pressure. The separation efficiency, E_{HC}, was determined based on the inlet and underflow oil concentration, using Eq. 3.10.

Because a non-commercial hydrocyclone was used, a series of commissioning tests were conducted to map the hydraulic and separation performances within the region of operation [2]. The commissioning tests were also conducted to study the effect of changing the hydrocyclone inlet pressure, as this is a consequence of varying the pumping pressure. Eq. 4.2 shows the obtained relationship between Q_{in}, the inlet flow rate (m^3/h), and Δp_{uf}, the underflow pressure drop (bar) [2]:

$$\Delta p_{uf} = p_m - p_d = 0.8 \cdot {Q_{in}}^{2.1}. \tag{4.2}$$

Comparison of the overflow flow rate, Q_o, accessed through the sample point shown in the right picture of Figure 4.9, and the inlet flow rate, Q_{in}, revealed the following relationship between the PDR, φ_{PDR}, and the flow split, F [2]:

$$F = \frac{Q_o}{Q_{in}} \cdot 100\ \% = \frac{\varphi_{PDR} - 1}{34} \cdot 100\ \%, \tag{4.3}$$

which was unaffected by changes in the inlet pressure and flow rate.

In addition to the hydraulic performance, the commissioning testing showed that the hydrocyclone had the same separation characteristics as expected form any deoiling hydrocyclone [2]. Most noteworthy for this project were the observations that the separation efficiency was neither affected by changes in the inlet pressure nor inlet oil concentration.

4.2.7 Control valves

Control valve CVo and CVd, seen in the right picture of Figure 4.9, were pneumatically spring-and-diaphragm actuator operated globe valves with microprocessor-based current-to-pneumatic valve positioners. The opening of CVo was controlled according to the desired PDR by a closed-loop PI-controller, while CVd was controlled according to the desired *upstream* pressure, p_u, also by a closed-loop PI-controller.

Manually operated needle valves were installed in parallel to bypass the control valves if necessary. The manual bypass valves are not shown in the schematics presented in Figure 4.2, but can be seen in the right picture of Figure 4.9. The control valve on the flow-control assembly, called CVs, was a globe valve with a multiple-spring diaphragm actuator and electro-pneumatic valve positioner. This valve was operated according to the desired sampling flow rate, Q_s, by a closed-loop PI-controller.

4.2.8 Vertical batch-separator

The vertical batch-separator was installed in parallel to the hydrocyclone as an alternative separation technology. This unit was only used in the test rig commissioning phase, and is, therefore, not included in the test rig schematics (Figure 4.2).

4.3 Fluid properties

Saltwater, with a salt concentration of 3.5 % (by weight), was prepared using tap water and heated to 50°C in the storage tank. The following combination of salts was used: $NaCl - 95.9$ %, $CaCl_2 - 3.2$ % and $MgCl_2 - 0.9$ %.

The density and viscosity characterized the oils used in the studies. The density was determined by the weight of a sample, divided by the sample volume, and the viscosity was determined using an Anton Paar Physica MCT 101 rheometer.

4.4 Instrumentation, communication, and control

Figure 4.10 shows schematics of the test rig signal communication layout. The center of communication was a programmable logic controller (PLC), sending control signals to the test rig equipment, and receiving measurements from the transmitters. Two personal computers (PCs) were used and are referred to as PC-A and PC-B, respectively. PC-A was the main PC, running the human–machine interface (HMI) and communicating with the Insitec. This PC was used throughout all investigations. PC-B ran the P&O-algorithms, and was, therefore, only used during the development and testing of these.

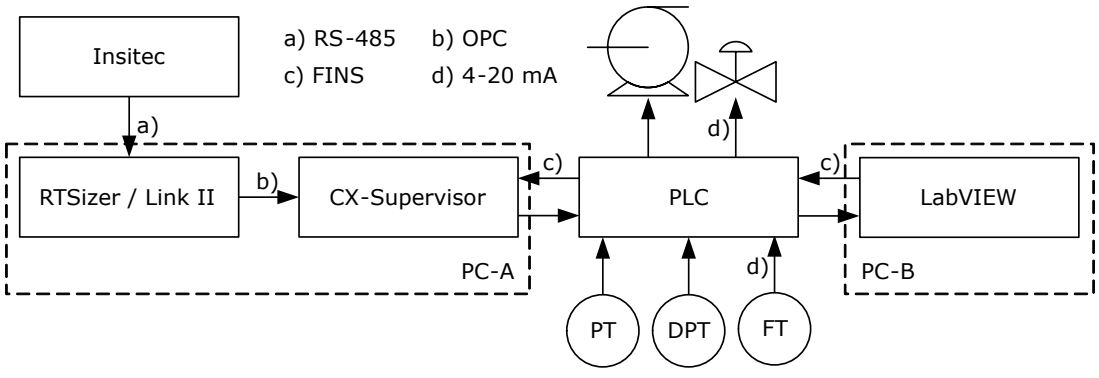

Figure 4.10: Schematics of the test rig signal communication layout.

4.4.1 PLC

The PLC was an OMRON SYSMAC CJ2M-CPU32, equipped with both digital and analog input and output expansion-units. The PLC received information from the flow and pressure transmitters and sent control signals to the VFDs and valve positioners via analog current loops ($4 - 20$ mA).

4.4.2 Flow and pressure transmitters

The test rig was equipped with two flow transmitters (FTs), both receiving measurements from magnetic flow meters; one of them was installed in the main test-section, downstream of the feeding pump, measuring Q_{u}, and the other in the flow-control assembly, measuring the sampling flow rate, Q_{s}. Pressure transmitters (PTs) and differential-pressure transmitters (DPTs) were installed throughout the test rig, reporting the pressures and differential pressures as required.

4.4.3 VFDs, valve positioners, and closed-loop controllers

The VFDs and valve positioners received control signals from the PLC based on the closed-loop PI-controllers shown in Figure 4.11, all of which were programmed into the PLC and tuned manually.

The set-point of the feeding pump, CVd, CVo, and CVs ($Q_{\mathrm{u}}^{\mathrm{SP}}$, $p_{\mathrm{u}}^{\mathrm{SP}}$, $\varphi_{\mathrm{PDR}}^{\mathrm{SP}}$, and $Q_{\mathrm{s}}^{\mathrm{SP}}$, respectively) were all controlled manually using the HMI. The coalescing-pump set-point, $\Delta p_{\mathrm{cp}}^{\mathrm{SP}}$, was either controlled manually or determined by a P&O-algorithm.

4.4.4 PC-A

The HMI was implemented into PC-A, using *CX-Supervisor*, and was used to control the test rig, communicating with the PLC via Factory Interface Network Service (FINS).

The Insitec measurements were first sent to PC-A via RS-485, received and analyzed by an application called *RTSizer*. *Link II*, another software application, further transferred selected parameters of the Insitec readings from RTSizer to CX-Supervisor via Open Platform Communications (OPC). From CX-Supervisor, the selected Insitec readings were further transferred to the PLC, via FINS, from which PC-B read and used them in the P&O-algorithms. In addition, Insitec droplet size distribution and oil concentration readings, analyzed by RTSizer, were stored in .txt files and post-processed using *Excel*.

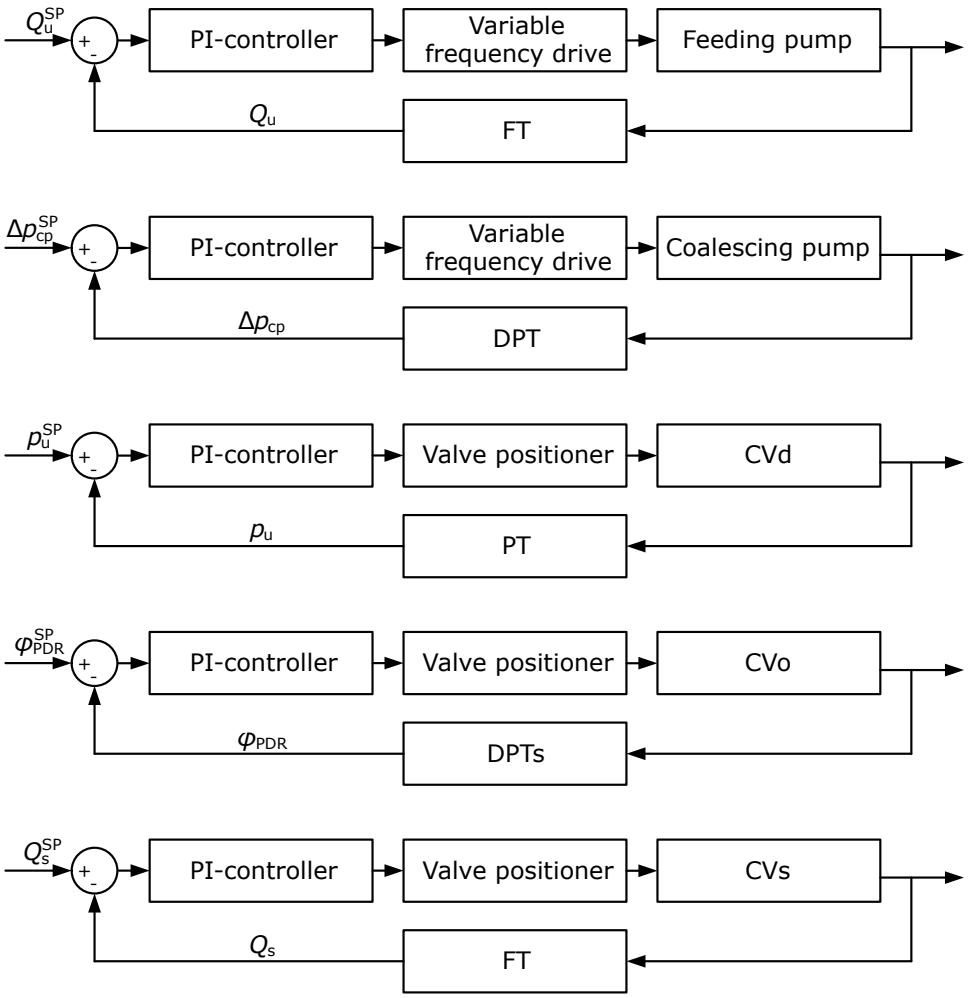

Figure 4.11: Schematics of the PI-controllers.

4.4.5 PC-B

LabVIEW was installed on PC-B and used to program and run the P&O-algorithms, communicating and receiving the required real-time parameters from the PLC via FINS. Further details of the P&O-algorithms are found in [3] and [4]. Note that in a field application, the P&O-algorithms may be implemented in the PLC, making PC-B obsolete.

Chapter 5

Main results and findings

In Chapter 1, the main hypothesis behind the work of this thesis was presented along with the subsequent four objectives. In the framework of the objectives, this chapter presents and discusses the main results and findings. Further details and discussions can be found in the appended papers. Figure 5.1 illustrates the physical units of focus the in experimental work done when elaborating the respective objectives.

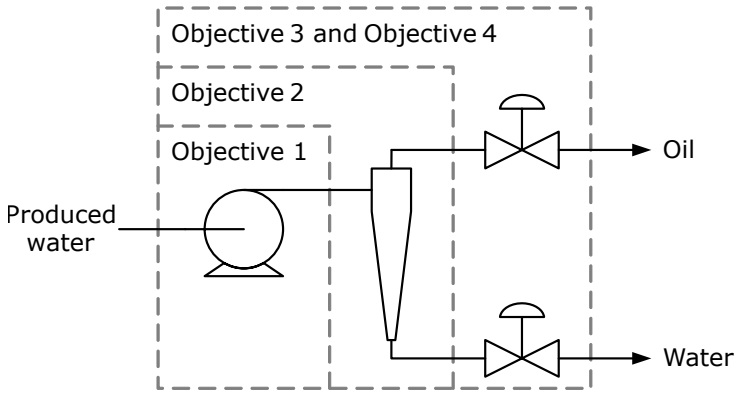

Figure 5.1: Illustration identifying the components in focus in the respective objectives.

For Objective 1, the focus was at the novel coalescing centrifugal pump. Objective 2 focused on both the coalescing pump and the hydrocyclone, while Objective 3 and Objective 4 focused on the whole system.

5.1 Results and findings from Objective 1

Objective 1 was to study the coalescing performance of the novel multistage centrifugal pump for produced water applications. Through this work, the initial observation that the coalescing effect is affected by the combination of pumping pressure and flow rate, introduced in Section 1.3.3, was verified.

Generally, it was found that [1]:

- Reducing the flow rate increased the coalescing effect.
- Reducing the size of the inlet droplets increased the coalescing effect; however, the largest outlet droplets were obtained with the largest inlets droplets, despite the reduced relative growth [2].
- Increasing the oil concentration increased the coalescing effect.
- For a constant flow rate, the coalescing effect had a concaved relationship to the pumping pressure.
- An operational point with the highest coalescing effect was observed and called the *optimal point of operation*.
- The optimal point of operation changed with respect to the inlet d_{v50}, oil type, and flow rate.
- Changing the oil concentration did not notably affect the optimal point of operation.
- It was concluded that the overall droplet behavior inside the pump is a combined result of turbulent droplet breakup and coalescence.

Section 5.1.1 through 5.1.3 are further elaborations of the experimental work leading to the above findings. References are made to the relevant papers, where additional information can be found.

5.1.1 Effect of point of operation

Figure 5.2 shows results from the study of how the point of operation affects the droplet growth. This figure consists of adapted versions of Figure 6 in [1] and Figure 2 in [2]. In the investigation, the inlet droplet size distribution and oil concentration were constant ($d_{\mathrm{v50,u}} = 5$ μm and $C_{\mathrm{u}} = 1500$ ppm), whereas the flow rate and pumping pressure were varied. The pressure upstream of the pump was $p_{\mathrm{u}} = 10$ bar, and a light crude oil ($\rho_{\mathrm{o}} = 796$ kg/m^3 and $\mu_{\mathrm{o}} = 2.5$ cP, at 20°C) was used.

The left plot in Figure 5.2 presents the percentage change of d_{v50}, denoted $\Delta d_{\mathrm{v50}}{}^{(\%)}$, through the pump when it was operated at various combinations of pumping pressure and flow rate. The x-axis shows the pumping pressure, Δp_{cp}, while the y-axis shows $\Delta d_{\mathrm{v50}}{}^{(\%)}$. Polynomial curves are fitted between the measurements. The plot shows that the droplet growth generally increased with reduced flow rate, regardless of the pumping pressure. This increased growth is expected to be a result of the droplet's increased residence time inside the pump, and the increased chances of droplet-droplet collisions and coalescence [1].

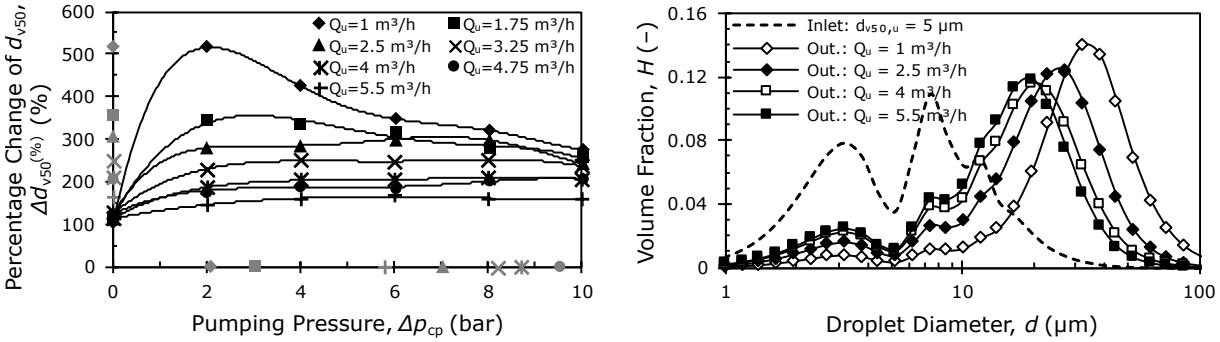

Figure 5.2: Left: Effect of point of operation [1]. Right: Inlet and outlet droplet size distribution for selected flow rates [2].

For a constant flow rate, it is seen that changing the pumping pressure also affects the droplet growth, forming a concaved relationship. This concaved shape is expected to be a result of a shift in the balance between the droplet-droplet coalescence and droplet breakup [1]. Initially, the droplet formation is characterized by coalescence-domination, increasing with increasing pumping pressure until a point where the coalescing effect starts to decrease [1]. Later results (Figure 5.3) show that high pumping pressures may result in droplet breakup-dominated behavior.

Due to the concaved relationship, a point of maximum droplet growth is obtained. This operational point is expected to promote the most beneficial combination of droplet-droplet coalescence and droplet breakup [1]. The left plot in Figure 5.2 shows that the optimal pumping pressure generally increased with increasing flow rate through the pump.

The right plot in Figure 5.2 shows the inlet and outlet droplet size distribution at $\Delta p_{\mathrm{cp}} = 4$ bar for selected flow rates. In the plot, the x-axis is a logarithmic scale with the various droplet diameters, while the y-axis is the volume fraction of each droplet size in the distributions. Again, it is seen that reducing the flow rate increases the droplet growth, as the volume fraction of small droplets is reduced while the fraction of large droplets increases [1].

5.1.2 Effect of inlet droplet size distribution

Figure 5.3 shows results from the study of how the inlet droplet size distribution affects the droplet growth. This figure shows adapted versions of Figure 7 and Figure 8 in [1]. During the investigation, the flow rate and oil concentration were constant ($Q_{\mathrm{u}} = 2.5$ m^3/h and $C_{\mathrm{u}} = 500$ ppm), whereas the inlet droplet size and pumping pressure were varied. The pressure upstream of the pump was $p_{\mathrm{u}} = 10$ bar. In the left plot, the light crude oil ($\rho_{\mathrm{o}} = 796$ kg/m^3 and $\mu_{\mathrm{o}} = 2.5$ cP, at 20°C) was used, whereas in the right plot, a medium crude ($\rho_{\mathrm{o}} = 882$ kg/m^3 and $\mu_{\mathrm{o}} = 27.2$ cP, at 20°C) was used.

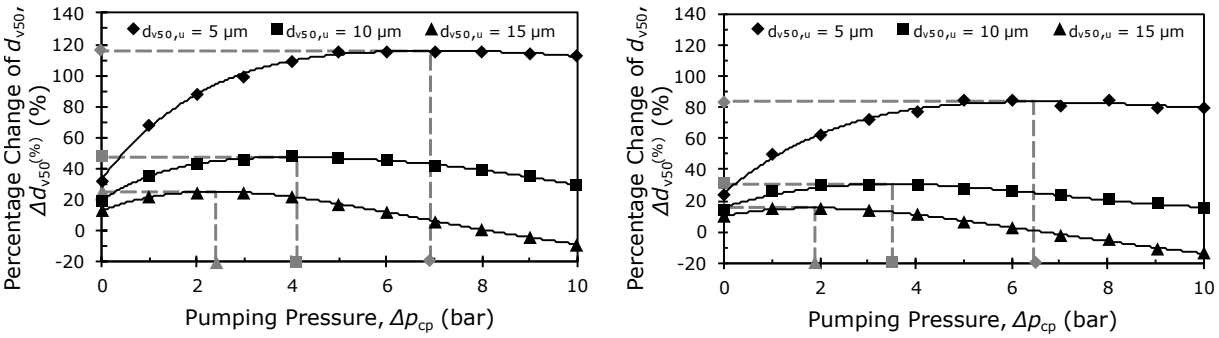

Figure 5.3: Left: Effect of inlet droplet size distribution, light crude [1]. Right: Effect of inlet droplet size distribution, medium crude [1].

Figure 5.3 shows that the inlet droplet size distribution affects both the relative droplet growth and the optimal point of operation. In general, increasing the inlet d_{v50} reduced $\Delta d_{\mathrm{v50}}{}^{(\%)}$ and the optimal pumping pressure [1]. As the inlet oil concentration was constant, the increased $d_{\mathrm{v50,u}}$ reduced the total number of droplets, further reducing the droplet-droplet collision frequency [1]. For some points of operation, a negative $\Delta d_{\mathrm{v50}}{}^{(\%)}$ was observed; this was only seen for large inlet droplets and high pumping pressure, and indicated that droplet breakup dominated over the coalescence [1].

For identical $d_{\mathrm{v50,u}}$ and point of operation, the left plot in Figure 5.3 shows higher droplet growth compared to that of the right plot, meaning that the lighter crude resulted in larger droplets [1]. Comparing the various points of operation, respectively, it is seen that the optimal pumping pressure is slightly higher for the light crude compared to that of the medium crude [1].

For further details regarding the effect of the inlet droplet size distribution, Figure 4 in [2] shows selected inlet and outlet droplet size distributions from each of the three light crude test series (left plot, Figure 5.3). From the figure, it can be seen that the largest outlet droplets were obtained with the largest inlet droplets, despite the reduced relative growth [2].

5.1.3 Effect of oil concentration

Figure 5.4 shows how changing the oil concentration affects the droplet growth. The figure contains plots adapted from Figure 9 and Figure 10 in [1]. In the investigation, the flow rate and inlet droplet size distribution were constant ($Q_{\mathrm{u}} = 2.5$ m^3/h and $d_{\mathrm{v50,u}} = 10$ μm), whereas the oil concentration and pumping pressure were varied. The pressure upstream of the pump was $p_{\mathrm{u}} = 10$ bar. In the left plot, the light crude oil ($\rho_{\mathrm{o}} = 796$ kg/m^3 and $\mu_{\mathrm{o}} = 2.5$ cP, at 20°C) was used, whereas in the right plot, the medium crude ($\rho_{\mathrm{o}} = 882$ kg/m^3 and $\mu_{\mathrm{o}} = 27.2$ cP, at 20°C) was used.

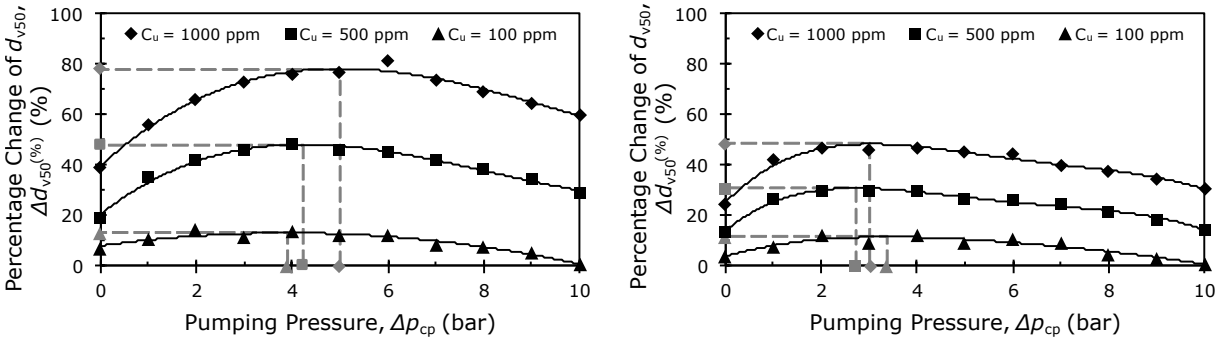

Figure 5.4: Left: Effect of oil concentration, light crude [1]. Right: Effect of oil concentration, medium crude [1].

Figure 5.4 shows that varying the oil concentration affects the droplet growth, where an increased oil concentration increased the coalescing effect [1]. As the inlet droplet size distributions are identical, an increased oil concentration increases the number of droplets. Logically, this in turns increases the droplet-droplet collision frequency, and coalescence activity [1].

With respect to the optimal pumping pressure, it is seen that changing the oil concentration had almost no effect [1]. Comparing the left and the right plot shows that the lighter crude resulted in greater droplet growth and higher optimal pumping pressure compared to that of the heavier crude [1].

For further details regarding the effect of the oil concentration, Figure 3 in [2] shows selected inlet and outlet droplet size distributions from each of the three light crude test series (left plot, Figure 5.4).

5.2 Results and findings from Objective 2

Objective 2 was to study the characteristics of the coalescing pump-hydrocyclone combination. In general [2]:

- The hydrocyclone separation efficiency was improved by the coalescing pump.
- Higher upstream oil concentrations resulted in greater improvements due to the increased coalescing effect.
- Increasing the oil concentration, having by-passed the coalescing pump, did not affect the separation efficiency.
- The separation efficiency was improved by increasing the size of the droplets upstream of the coalescing pump.

To model the interaction between the coalescing pump and the hydrocyclone, and to aid in the development of the considered control strategies, the hydrocyclone separation efficiency was studied with respect to the pumping pressure. Through this investigation, it was found that [2]:

- Solely changing the hydrocyclone inlet pressure, having bypassed the coalescing pump, did not affect the separation efficiency.
- Including the coalescing pump and varying the combination of pumping pressure, oil concentration, and pump inlet droplet size distribution, affected the coalescing effect and the resulting separation efficiency.
- A concaved relationship was observed between the pumping pressure and the downstream separation efficiency.
- The highest separation efficiency was achieved when the pump minimized the volume fraction of droplets smaller than the hydrocyclone cut size [2, 3].
- An empirical model was developed, predicting the optimal pumping pressure based on measurements of produced water characteristics upstream of the pump [3].

Section 5.2.1 through 5.2.3 are further elaborations of the experimental work leading to the above findings. References are made to the relevant papers, where additional information can be found.

5.2.1 Benefits of pumping pressure optimization

To study the benefits of optimizing the point of operation with respect to the downstream separation efficiency, three different produced water characteristics (PWCs) were used, representing various operational scenarios. The PWCs consisted of different combinations of oil concentration and inlet droplet size distribution, and were called PWC-01, PWC-02 and PWC-03. Similar for all scenarios where the oil type ($\rho_o = 779$ kg/m^3 and $\mu_o = 4.1$ cP, at 20°C), flow rate ($Q_u = 1.75$ m^3/h), the PDR ($\varphi_{PDR} = 1.7$) and the pressure upstream of the pump ($p_u = 10$ bar). Table 5.1 shows an adapted version of Table 2 in [2], listing the $d_{v50,u}$ and C_u for the three scenarios, respectively.

	PWC-01	PWC-02	PWC-03
$d_{v50,u}$ (μm)	5	5	15
C_u (ppm)	200	850	850

Table 5.1: Properties of PWC-01, PWC-02 and PWC-03 [2].

Figures 5.5 through 5.7 show results from the three scenarios. These figures are adapted versions of Figures 6 through 8 in [2]. Each figure consists of two plots; the left plot presents the coalescing pump inlet and outlet droplet size distribution corresponding to every second pressure increment. Here, the x-axis is a logarithmic scale with the various droplet diameters, and the y-axis is the volume fraction of each droplet size in the distributions. The dotted curve represents the inlet distribution, whereas the other curves represent outlet distributions. The right plots show the hydrocyclone separation efficiency. Here, the x-axis is the pumping pressure, while the y-axis is the hydrocyclone separation efficiency. Polynomial curves are added to highlight the trends.

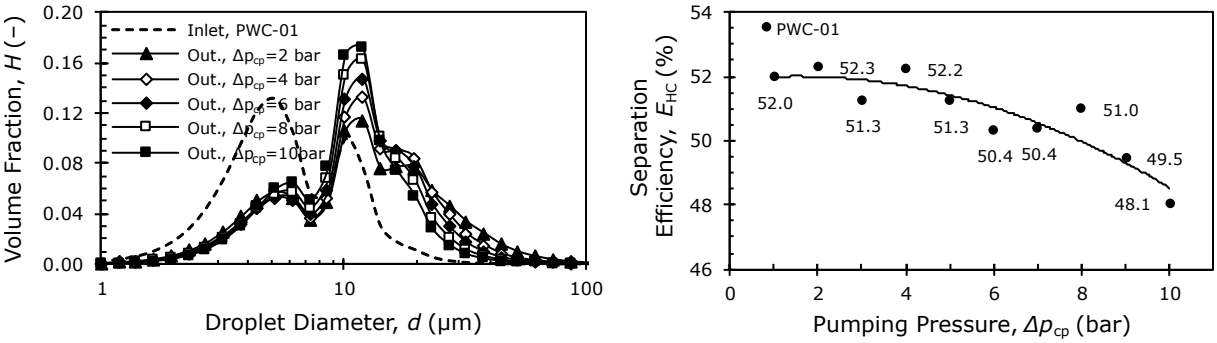

Figure 5.5: Left: PWC-01 inlet and outlet droplet size distribution [2]. Right: PWC-01 hydrocyclone separation efficiency [2].

Figure 5.5 shows the results of PWC-01; the left plot demonstrates how the coalescing pump reduced the volume fraction of the small droplets and consequently increased the volume fraction of larger droplets [2]. During the investigation, the cut-size of the hydrocyclone was estimated to $d_{50} = 10$ μm [2]. It is, therefore, seen that a significant portion of the droplets smaller than the cut-size has coalesced and formed larger droplets, increasing their chance of separation [2]. In the right plot, the optimal pumping pressure is observed between 1 and 4 bar, where a higher pumping pressure reduces the separation efficiency [2].

Figure 5.6 shows results from PWC-02, where the left plot shows increased droplet growth compared to that of Figure 5.5. As discussed in Section 5.1.3, the increased droplet growth is probably due to the increased coalescence activity, having a higher oil concentration compared to that of PWC-01 [2]. By comparing the outlet droplet size distributions in Figure 5.6, it is seen that the distributions tend to narrow as the pumping pressure is increased [2]. Consequently, the size of the largest droplets decreases, increasing the volume fraction of droplets with a diameter of around 20 μm. The right plot of Figure 5.6 demonstrates the concaved relationship between the pumping pressure and the separation efficiency [2]. A rapid increase in the separation efficiency with increasing pumping pressure is seen, having a maximum efficiency plateau between 4 and 6 bar.

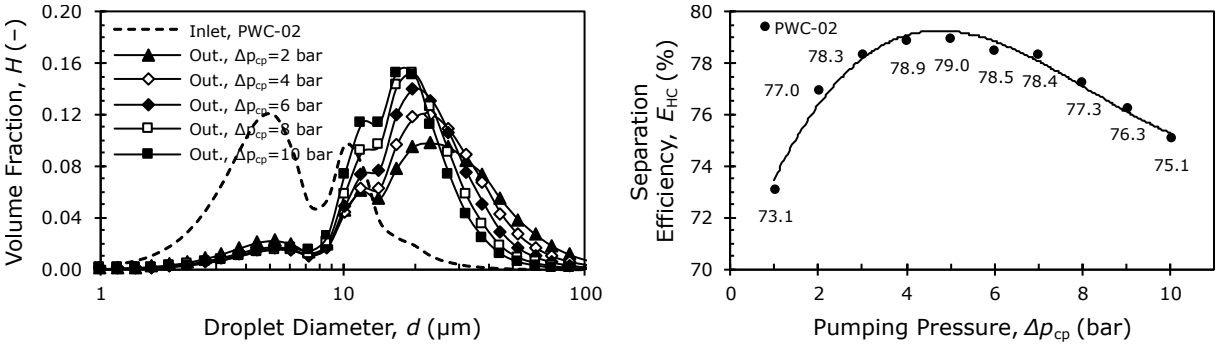

Figure 5.6: Left: PWC-02 inlet and outlet droplet size distribution [2]. Right: PWC-02 hydrocyclone separation efficiency [2].

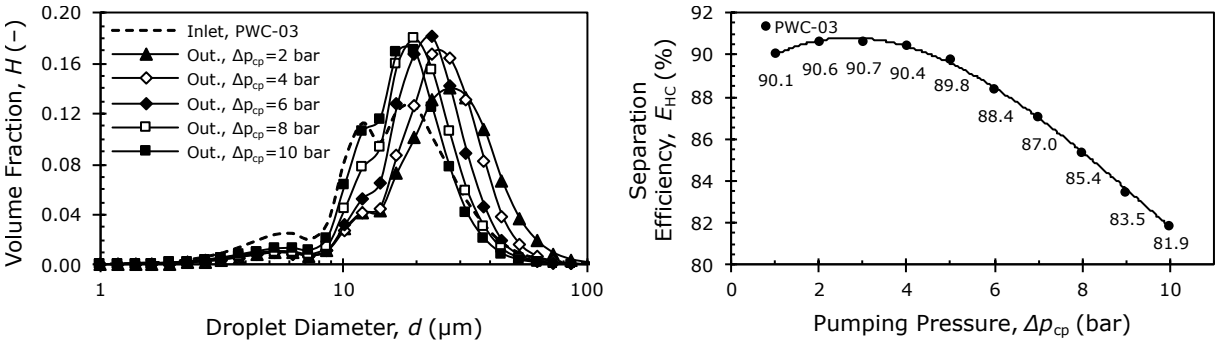

Figure 5.7: Left: PWC-03 inlet and outlet droplet size distribution [2]. Right: PWC-03 hydrocyclone separation efficiency [2].

Beyond 6 bar pumping pressure, the separation efficiency declines.

Figure 5.7 shows results from PWC-03. In this scenario, the volume fraction of small droplets in the inlet distribution was low compared to that of PWC-01 and PWC-02, and the growth of these was therefore not as distinct [2]. The same narrowing tendency with increasing pumping pressure is seen in the left plot. The right plot demonstrates the same concaved relationship, having a peaked separation efficiency at around 3 bar pumping pressure [2].

5.2.2 Effect of oil type

Testing with various oil types was conducted to study how crude properties affected the coalescence and separation characteristics, and to compare the use of Exxsol to that of real crude oil. Four stabilized crude oils, and one Exxsol were used. All oils were injected in a concentration of $C_{\mathrm{u}} = 600$ ppm and mixed so that the volume median droplet diameter was $d_{\mathrm{v50,u}} = 11$ μm upstream of the coalescing pump. The flow rate was $Q_{\mathrm{u}} = 1.75$ m^3/h, the PDR was $\varphi_{\mathrm{PDR}} = 2$ and the pressure upstream of the pump was $p_{\mathrm{u}} = 10$ bar. Table 5.2 shows an adapted version of Table 1 in [3], listing the oil properties.

Oil	ρ_o (kg/m^3)	μ_o (cP)
Exxsol D140	824	6.14
Crude A	814.5	4.9
Crude B	837.5	5.6
Crude C	862.5	13.0
Crude D	891.5	29.3

Table 5.2: Oil properties [3].

Figure 5.8 shows results from the investigation, consisting of adapted versions of Figure 8 and Figure 9 in [3]. In Figure 5.8, the left plot shows the hydrocyclone separation efficiency (y-axis) relative to the pumping pressure (x-axis). The right plot shows the pump effluent droplet size distribution at the optimal point of operation for each of the five oils, respectively. Here, the x-axis is a logarithmic scale with the various droplet diameters, and the y-axis is the volume fraction of each droplet size.

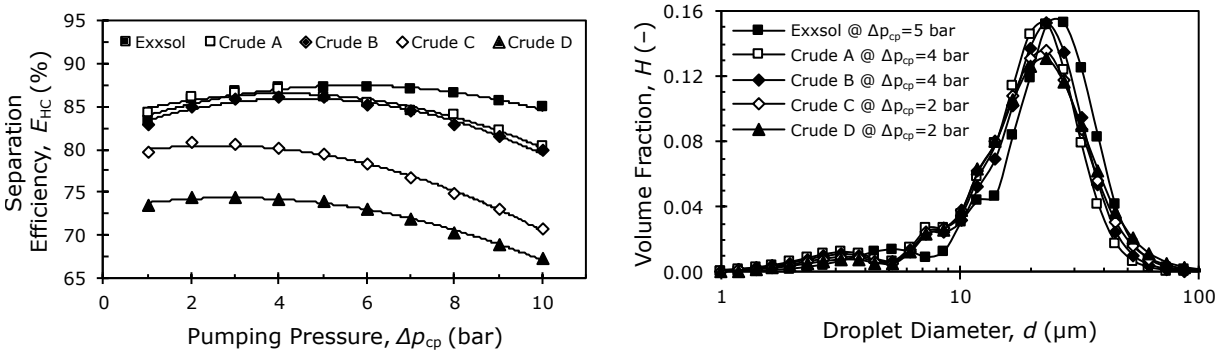

Figure 5.8: Left: Separation efficiency using various oils [3]. Right: Pump outlet droplet size distribution at the optimal point of operation [3].

The left plot of Figure 5.8 shows that the point of operation had the same characteristic effect on the separation of Exxsol as for the crude oils, showing the same concaved relationship and distinct optimal pumping pressure [3]. At low pumping pressures, the lightest crude (Crude A) had the highest separation efficiency, and the efficiency decreased with increasing density [3]. At higher pumping pressures, however, the Exxsol gave an even higher separation efficiency, despite being the second lightest oil [3]. The right plot shows that the droplets at the pump outlet, when operated at the optimal pumping pressure, were similarly distributed for all oils, including the Exxsol [3].

Table 5.3 shows an adapted version of Table 4 in [3], listing the optimal pumping pressure, Δp_{opt}, and resulting separation efficiency, $E_{HC}@\Delta p_{opt}$, for all the investigated oils, respectively.

From the table, it is seen that, generally, both the optimal pumping pressure and the

Oil	Δp_{opt} (bar)	$E_{\text{HC}}@\Delta p_{\text{opt}}$
Exxsol D140	5	87.3 %
Crude A	4	86.9 %
Crude B	4	86.1 %
Crude C	2	80.7 %
Crude D	2	74.5 %

Table 5.3: Optimal pumping pressure and highest separation efficiency [3].

resulting separation efficiency declined with increasing density and viscosity [3]. Only the Exxsol deviated slightly from this trend by having the highest separation efficiency and the highest optimal pumping pressure [3]. Nonetheless, as the Exxsol gave the same characteristics results as the crude oils, and due to practicality and availability, this oil was used throughout the following testing and investigations.

5.2.3 Overall trends and modeling

To study overall trends, and to develop an empirical model predicting the optimal pumping pressure based on upstream measurements, 24 test series were conducted using Exxsol. The tests consisted of 16 series for modeling and 8 series for verification. The 16 modeling series were made out of various combinations of inlet oil concentrations and droplet size distributions, where $C_{\text{u}} = \{200,\ 400,\ 600,\ 800\}$ ppm and $d_{\text{v50,u}} = \{7.5,\ 10,\ 12.5,\ 15\}$ μm. For the 8 verification series, $C_{\text{u}} = \{200,\ 400,\ 600,\ 800\}$ ppm and $d_{\text{v50,u}} = \{11,\ 18\}$ μm. In all tests, the flow rate was $Q_{\text{u}} = 1.75$ m^3/h, the PDR was $\varphi_{\text{PDR}} = 2$ and the pressure upstream of the pump was $p_{\text{u}} = 10$ bar.

Figure 5.9 shows adapted versions of Figure 10 and Figure 13 in [3]. In the left plot, the hydrocyclone separation efficiency at the optimal point of operation, $E_{\text{HC}}@\Delta p_{\text{opt}}$, is shown for all test series, including both the series for modeling and verification. Here, the x-axis shows d_{v50} of the droplet size distribution entering the pump, while the y-axis shows $E_{\text{HC}}@\Delta p_{\text{opt}}$. The various oil concentrations are marked with different symbols, and straight lines are drawn between the data points. In addition, the hydrocyclone separation efficiency measured when bypassing the coalescing pump, is included as a reference. As mentioned in Section 4.2.6, changing the upstream oil concentration while bypassing the pump does not affect the hydrocyclone separation efficiency [2]; these results are therefore forming a single line. The right plot shows the measured separation efficiency (y-axis) compared to the droplet size distribution entering the hydrocyclone (x-axis). Here, hydrocyclone inlet droplet size distribution is characterized by its total volume fraction of droplet larger than d_{lim}, denoted $\%V_{\text{d>d}_{\text{lim}}}$.

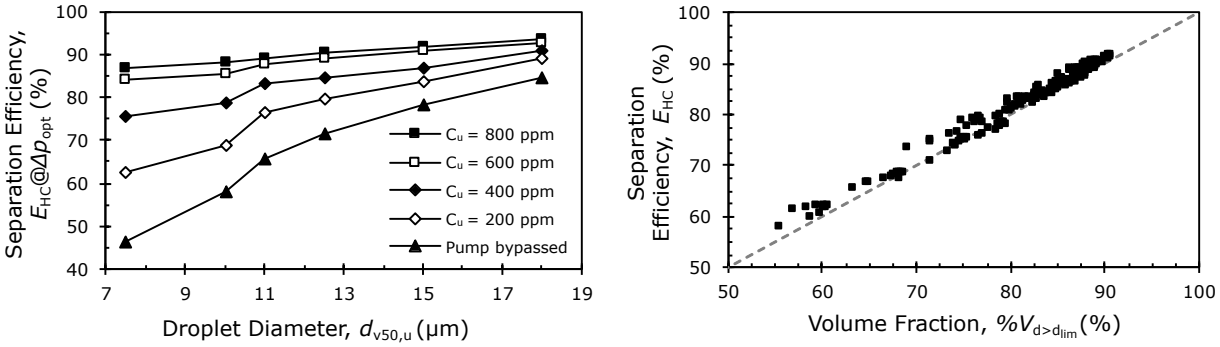

Figure 5.9: Left: Hydrocyclone separation efficiency [3]. Right: Comparison of hydrocyclone separation efficiency and inlet droplet size distribution [3].

The left plot in Figure 5.9 shows that while having the pump operating at the optimal pumping pressure, the resulting separation efficiency increases with increased inlet droplet size and oil concentration [3]; these trends are in accordance with the characteristics of the coalescing effect discussed in Section 5.1.2 and Section 5.1.3, respectively. The right plot shows an observed relationship between the droplet size distribution entering the hydrocyclone, i.e., leaving the pump, and the resulting separation efficiency. The limit size was set to $d_{\text{lim}} = 11$ μm, and the plot shows that $\%V_{\text{d>d}_{\text{lim}}}$ was approximately equal to the resulting separation efficiency [2, 3]. This observation was the background for the simplified hydrocyclone separation efficiency estimation method discussed in Section 3.2.3.

Figure 5.10 shows adapted versions of Figure 11 and Figure 12 in [3]. In the left plot, the optimal pumping pressure (y-axis) for the 16 modeling test series are shown with respect to the upstream oil concentration (x-axis) for various $d_{\text{v50,u}}$. The plot also shows the average value of the optimal pumping pressures for each of the different $d_{\text{v50,u}}$, denoted Δp_{avg}. The right plot shows an empirical model (dotted line) made out of the results presented in the left plot. Here, the x-axis shows $d_{\text{v50,u}}$, while the y-axis shows Δp_{avg}. The black squares mark the modeling data, while the white squares mark the verification data.

The left plot in Figure 5.10 shows that, generally, the optimal pumping pressure decreased with increasing $d_{\text{v50,u}}$ [3]. The oil concentration had some influence; however, to a lesser extent and without any obvious trend. Therefore, and for simplicity, the empirical model was made based on the assumption that changes in the upstream oil concentration did not affect the optimal pumping pressure [3]. To exclude C_{u} as a model parameter, the average optimal pumping pressure for each value of the $d_{\text{v50,u}}$, Δp_{avg}, was used as modeling and verification data. The empirical model was defined as [3]:

$$\Delta p_{\text{pre}} = \kappa \cdot {d_{\text{v50,u}}}^{b}, \tag{5.1}$$

where $\kappa = 48.71$ $\frac{\text{bar}}{\mu\text{m}^b}$ and $b = -0.95$. Δp_{pre} is the predicted optimal pumping pressure.

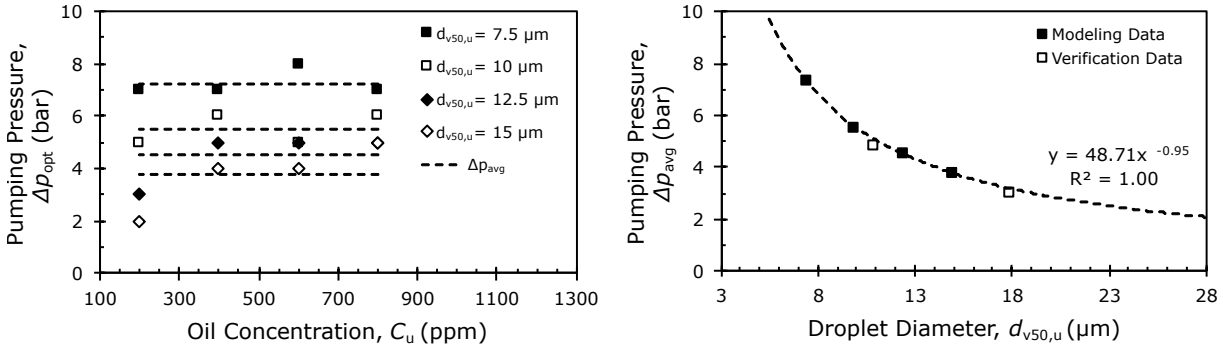

Figure 5.10: Left: Optimal pumping pressure for various PWCs [3]. Right: Empirical model for optimal pumping pressure prediction [3].

5.3 Results and findings from Objective 3

Objective 3 were to implement and study the considered control strategies presented in Section 1.4, based on three different analyzer positions. It was found that [3]:

- The *midstream* and *downstream* positions were the most comparable as both required process feedback and employed P&O-algorithms.
- An analyzer in the *upstream* position required neither feedback nor a P&O-algorithm, as this method *predicted* the optimal pumping pressure.
- The *upstream* location will most likely result in the quickest reaction to process changes, but is at the same time highly dependent on the accuracy of the coalescing pump/hydrocyclone performance model.
- The *midstream* position required only an accurate model of the hydrocyclone separation, and therefore lacked the uncertainties introduced by a model of the coalescing pump.
- The *downstream* position did not require any prior knowledge of neither the pump nor the separation equipment, as it was solely based on the resulting downstream oil concentration.
- The *downstream* position may result in the slowest reaction time of the three, as the measured process parameter is most distant from the pump, but it is at the same time the only method adjusting the pump operation based on the actual performance, without introducing any predictions.
- Overall, the *downstream* position was considered the best approach for most applications due to the robustness and ease of implementation.

Section 5.3.1 through 5.3.4 are further elaborations of the experimental work leading to the above findings. References are made to the relevant papers, where additional information can be found.

5.3.1 Implementation of the *upstream* oil-in-water analyzer

The control strategy having an oil-in-water analyzer in the *upstream* position, was introduced in Section 1.4.1. The concept is to use the empirical model presented in Eq. 5.1 to predict the optimal pumping pressure of the coalescing pump. This model requires continuous measurements of $d_{\mathrm{v50,u}}$, which is provided by the upstream analyzer. In the following investigation, this method of control will be discussed based on the pumping pressure it predicts and will be used as a reference for the two tracking strategies.

5.3.2 Implementation of the *midstream* oil-in-water analyzer

In the *midstream* position, the oil-in-water analyzer measures the characteristics of the produced water between the coalescing pump and the deoiling hydrocyclone. The concept is to use the coalescing pump to manipulate the droplet size distribution, shaping it to optimize the hydrocyclone separation efficiency. This strategy was introduced in Section 1.4.2, and employs the concaved relationship between the pumping pressure and resulting separation efficiency, using P&O-algorithms to approach the optimal point of operation.

Section 3.2.3 introduced a simplified method to estimate the hydrocyclone separation efficiency based on the inlet droplet size distribution. With the analyzer in the *midstream* position, this method was used to determine the coalescing pump point of operation. In the implementation of this strategy, a P&O-algorithm was developed. A general introduction of P&O-algorithms was given in Section 1.4.4, whereas further details of the implemented algorithm can be found in [3]. The algorithm adjusted the pumping pressure to minimize $\%V_{\mathrm{d<d_{lim}}} = (100\ \% - \%V_{\mathrm{d>d_{lim}}})$, which is the volume fraction of droplets *smaller* than the predetermined limit, d_{lim}. Thereby, the controller minimized the volume fraction of droplets assumed to be too small to be removed by the hydrocyclone [3]. The limit size was set to $d_{\mathrm{lim}} = 11\ \mu$m.

5.3.3 Implementation of the *downstream* oil-in-water analyzer

In the *downstream* position, the oil-in-water analyzer was used to measure the oil concentration at the hydrocyclone underflow outlet, i.e., the concentration of oil in the cleaned water. This control strategy was first presented in Section 1.4.3, and involves the use of

a P&O-algorithm to track the pumping pressure resulting in the lowest downstream oil concentration. Further details of the implemented algorithm can be found in [3].

5.3.4 Comparative testing and discussions

Figure 5.11 is an adapted version of Figure 14 in [3], and shows results from the testing with the oil-in-water analyzer in the *midstream* position. The figure consists of four plots, showing the results from one of four trail runs; Table 5.4 lists C_{u} and $d_{\mathrm{v50,u}}$ for each of the tests. During the testing, the flow rate was $Q_{\mathrm{u}} = 1.75$ m^3/h, the PDR was $\varphi_{\mathrm{PDR}} = 2$, the upstream pressure was $p_{\mathrm{u}} = 10$ bar, and the pumping pressure was changed by the P&O-algorithm in steps of $\delta_{\Delta\mathrm{p}} = 1$ bar. In the plots, the x-axis shows the time, while the left y-axis shows the final value of $\%V_{\mathrm{d<d_{lim}}}$ for each iteration of the P&O-algorithm. The right y-axis shows the pumping pressure, and the optimal pumping pressure predicted by the empirical model (Eq. 5.1) is included as a dotted line, for comparison.

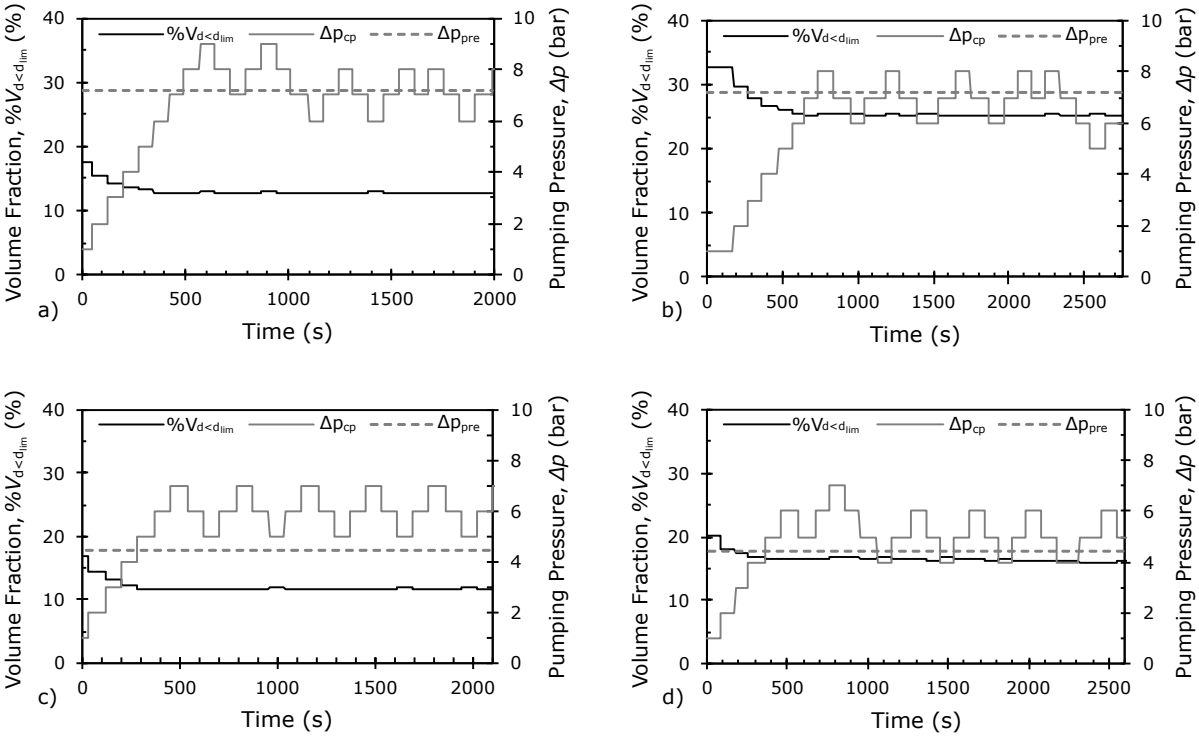

Figure 5.11: Test results having the oil-in-water analyzer in the *midstream* position [3].

Plot:	a)	b)	c)	d)
$d_{\mathrm{v50,u}}$ (μm)	7.5	7.5	12.5	12.5
C_{u} (ppm)	800	400	800	400

Table 5.4: Produced water characteristics for the various trail runs [3].

Figure 5.12 shows an adapted version of Figure 15 in [3]. This figure shows test results having the oil-in-water analyzer placed in the *downstream* position. The produced water characteristics for each plot were equal to those of Figure 5.11, respectively. In each plot, the x-axis shows the time, and the left y-axis shows the measured downstream oil concentration, C_{d}. The right y-axis shows the pumping pressure, and Δp_{pre} is included for comparison.

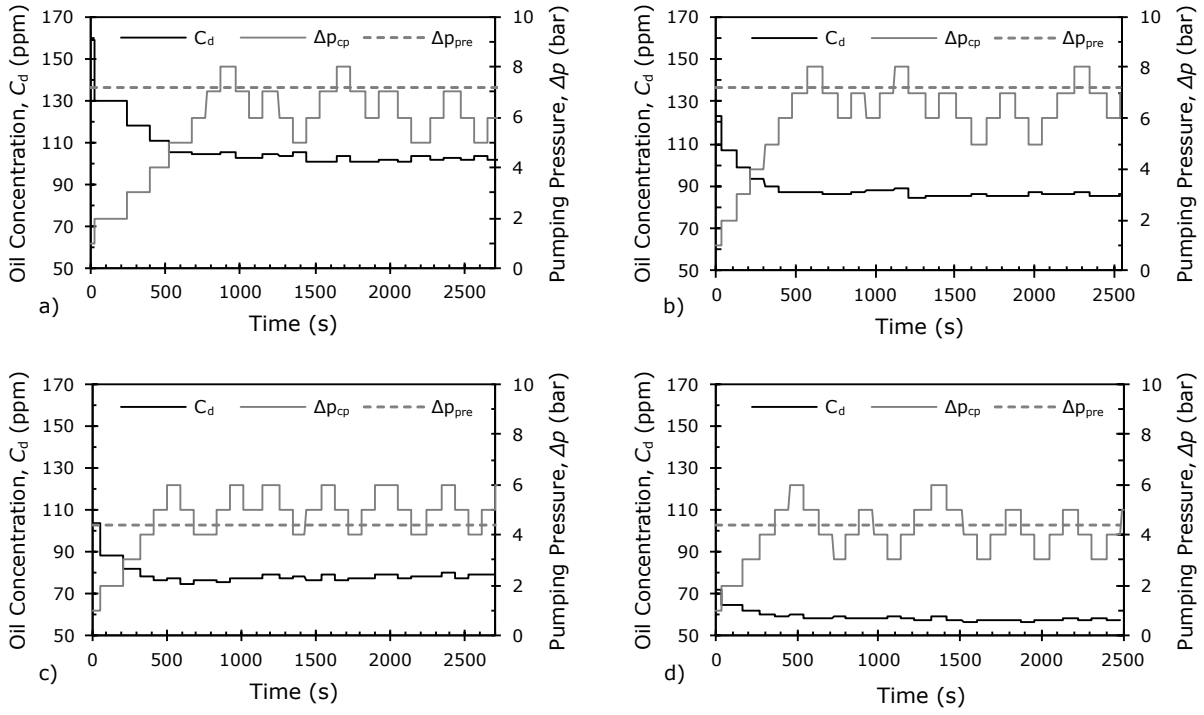

Figure 5.12: Test results having the oil-in-water analyzer in the *downstream* position [3].

Table 5.5 is made out of data from Table 5 and Table 6 in [3], and shows the resulting separation efficiency estimated for the two tracking methods. Having the oil-in-water analyzer in the *downstream* position, the separation efficiency was estimated using Eq. 3.10. With the analyzer in the *midstream* position, the separation efficiency was estimated using Eq. 3.13.

Plot:	a)	b)	c)	d)
Figure 5.11 (*midstream*), E_{HC}:	87 %	75 %	88 %	84 %
Figure 5.12 (*downstream*), E_{HC}:	88 %	79 %	90 %	86 %

Table 5.5: Resulting hydrocyclone separation efficiency for the two tracking methods [3].

Table 5.5 shows that both tracking methods resulted in more or less the same separation efficiency for each respective trail run [3]. For further details, each trail run is discussed more thoroughly in [3]. Generally, both tracking methods approached the pump-

ing pressure predicted by the empirical model, indicating that any of the three control strategies may be used to optimize the pumping pressure [3].

In the investigation, produced water characteristics such as temperature and salinity, oil type, viscosity and density, and process related properties such as flow rate and upstream pressure were all fixed, and therefore not included as variables in the empirical model. To successfully implement the model-prediction method in a real application, all varying properties that may affect the optimal point of operation must be included as model variables and measured in real-time. Also, the modeling and measurements must be cost-efficient and robust for this strategy to be realistic. Having the oil-in-water analyzer in the *midstream* position involves model-prediction of the hydrocyclone separation. The implementation method suggested in this investigation should, therefore, be expanded to include varying properties not already considered in the current model. The control strategy involving the *downstream* oil-in-water analyzer does not include model-prediction. Therefore, and due to its robustness and ease of implementation, this method was concluded as the recommended approach [3].

5.4 Results and findings from Objective 4

Objective 4 was to improve the control strategy recommended by the activities couplet to Objective 3, where it was concluded that tracking based on the measurements of a *downstream* oil-in-water analyzer was the most robust and reliable approach [3]. General drawbacks of P&O-algorithm were discussed Section 1.4.4.

In this study [4]:

- Three variable step size P&O-algorithms were developed and introduced to reduce the response time, in addition to reducing (or eliminating) steady-state oscillations.
- Simulations and experimental testing were conducted to highlight and discuss the advantages and disadvantages of the three variable step size P&O-algorithms.
- The basic variable step size (BVSS) P&O-algorithm had a weakness toward rapid environmental changes, as it possessed the risk of stepping away from the new optimal pumping pressure, rather than toward it.
- To avoid stepping astray, the hybrid variable step size (HVSS) and the triggered variable step size (TVSS) P&O-algorithm introduced a probe step.

- The HVSS P&O-algorithm was characterized by continuously tracking the optimal point of operation, while the TVSS P&O-algorithms stayed dormant for most of the time.
- It was concluded that the constant steady-state pumping pressure of the TVSS P&O-algorithm must be weighed against the continuous tracking of the HVSS P&O-algorithm, depending on whether steady or drifting environmental conditions are expected.

Section 5.4.1 through 5.4.3 are further elaborations of the experimental work leading to the above findings. References are made to the relevant papers, where additional information can be found.

5.4.1 Variable step size

The variable step size was related to the relative change in downstream oil concentration by the following equation [4]:

$$\delta_{\Delta \mathrm{p,n}} = \frac{K}{\bar{C}_{\mathrm{d,n}}} \cdot \frac{|C_{\mathrm{d,n}} - C_{\mathrm{d,n\text{-}1}}|}{|\Delta p_{\mathrm{cp,n}} - \Delta p_{\mathrm{cp,n\text{-}1}}|}, \tag{5.2}$$

where $\delta_{\Delta \mathrm{p,n}}$ is the step size, K is a tuning parameter (also called *controller gain*), $C_{\mathrm{d,n}}$ and $C_{\mathrm{d,n\text{-}1}}$ are the current and previous downstream oil concentration, $\Delta p_{\mathrm{cp,n}}$ and $\Delta p_{\mathrm{cp,n\text{-}1}}$ are the current and previous pumping pressure, and n is the current iteration number of the P&O-algorithm. $\bar{C}_{\mathrm{d,n}}$ is the mean value of $C_{\mathrm{d,n}}$ and $C_{\mathrm{d,n\text{-}1}}$, and is determined as follows [4]:

$$\bar{C}_{\mathrm{d,n}} = \frac{C_{\mathrm{d,n}} + C_{\mathrm{d,n\text{-}1}}}{2}. \tag{5.3}$$

By defining the previous pumping pressure step as $\delta_{\Delta \mathrm{p,n\text{-}1}} = |\Delta p_{\mathrm{cp,n}} - \Delta p_{\mathrm{cp,n\text{-}1}}|$, and introducing $N = |C_{\mathrm{d,n}} - C_{\mathrm{d,n\text{-}1}}|/\bar{C}_{\mathrm{d,n}}$, Eq. 5.2 was simplified to [4]:

$$\delta_{\Delta \mathrm{p,n}} = K \cdot \frac{N}{\delta_{\Delta \mathrm{p,n\text{-}1}}}. \tag{5.4}$$

In addition, a saturation was introduced so that

$$\delta_{\Delta \mathrm{p,n}} \in \left[\delta_{\Delta \mathrm{p}}^{(\mathrm{min})},\ \delta_{\Delta \mathrm{p}}^{(\mathrm{max})}\right], \tag{5.5}$$

where $\delta_{\Delta \mathrm{p}}^{(\mathrm{min})}$ and $\delta_{\Delta \mathrm{p}}^{(\mathrm{max})}$ are the minimum and maximum allowable step size [4]. The limits were included to make sure the pumping pressure perturbation observably affected the downstream oil concentration, and to limit the maximum pumping pressure change [4].

It was emphasized that the controller gain K should be determined for each specific application and pump, and it was suggested that the gain was tuned according to the two following properties [4];

1. reducing the amplitude of the pumping pressure changes to stabilize the system during steady-state operations, and
2. minimizing the amount of oil exiting the hydrocyclone underflow by rapidly responding to abrupt changes in the upstream produced water characteristics.

The two properties were mathematically defined as [4]:

$$\min R_1, \tag{5.6}$$

where

$$R_1 = \sum_{i=1}^{n} \left| \delta_{\Delta \mathrm{p,i}} \right|, \tag{5.7}$$

and

$$\min R_2, \tag{5.8}$$

where

$$R_2 = \sum_{i=1}^{n} \left| C_{\mathrm{d,i}} \cdot \Delta t_{\mathrm{i}} \right|, \tag{5.9}$$

and Δt is the step time. Also, a method of estimating an adequate value of K was presented in [4], in addition to a discussion of the effect of adjusting the gain.

Following are results from the experimental testing of the BVSS P&O-algorithm. During the testing, the system initially started in steady-state, encircling the current optimal pumping pressure. Then, a sudden change in the upstream produced water characteristics was introduced in the form of a change in the droplet size distribution, also shifting the optimal pumping pressure. After the change, the environmental conditions were again kept constant as the system adapted to the new conditions. During the testing, the flow rate was $Q_{\mathrm{u}} = 1.75$ m^3/h, the PDR was $\varphi_{\mathrm{PDR}} = 2$, the upstream pressure was $p_{\mathrm{u}} = 10$ bar, the upstream oil concentration was $C_{\mathrm{u}} = 400$ ppm, and the Exxsol was used. The minimum pumping pressure step size was $\delta_{\Delta \mathrm{p}}^{(\mathrm{min})} = 0.25$ bar and the maximum was $\delta_{\Delta \mathrm{p}}^{(\mathrm{max})} = 2$ bar. The upstream d_{v50} was initially $d_{\mathrm{v50,u}} = 12.5$ μm and shifted to $d_{\mathrm{v50,u}} = 7.5$ μm.

Figures 5.13 through 5.15 show adapted versions of Figure 7 through 9 in [4]. The figures contain two plots each, where the left plot shows the pumping pressure (y-axis) as a function of time (x-axis), while the right plot shows the downstream oil concentration (y-axis) as a function of time (x-axis). The left plot also shows the model predicted optimal pumping pressure, Δp_{pre}. In both plots, the environmental change is indicated by a change in the background color.

The three experimental tests were distinguished by the value of controller gain, K; the three gains were $K = 0.1$ bar^2, $K = 10$ bar^2 and $K = 100$ bar^2. Table 5.6 is an adapted

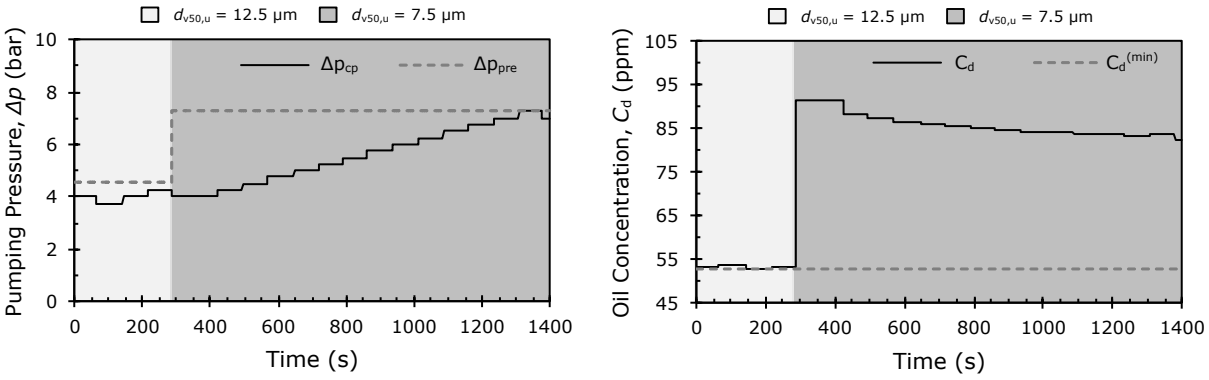

Figure 5.13: Experimental testing of the BVSS P&O-algorithm with $K = 0.1$ bar^2 [4].

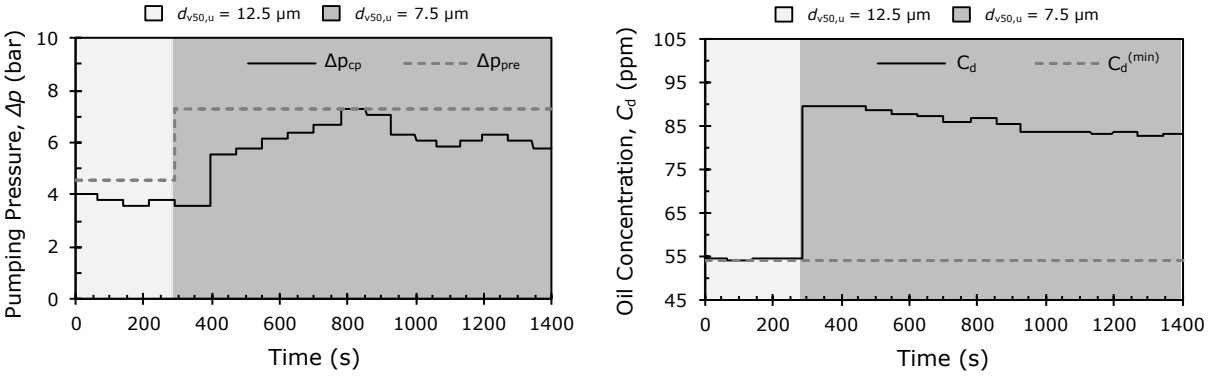

Figure 5.14: Experimental testing of the BVSS P&O-algorithm with $K = 10$ bar^2 [4].

version of Table 1 in [4], listing the resulting R_1' and R_2' for the three experimental tests. R_1' and R_2' are R_1 and R_2 rescaled to the range $[0,\ 1]$, as follows [4]:

$$R_1' = \frac{R_1 - \min R_1}{\max R_1 - \min R_1}, \tag{5.10}$$

$$R_2' = \frac{R_2 - \min R_2}{\max R_2 - \min R_2}. \tag{5.11}$$

Note that $C_{\mathrm{d,i}}$ in Eq. 5.9 was replaced with $\left(C_{\mathrm{d,i}} - C_{\mathrm{d}}^{(\min)}\right)$, where $C_{\mathrm{d}}^{(\min)}$ is the lowest oil concentration measured downstream of the hydrocyclone during each test, respectively, and is included in the right plots. This modification was done to compensate for experimental differences, ensuring fair comparison between the three tests [4].

	$K = 0.1$ bar^2	$K = 10$ bar^2	$K = 100$ bar^2
R_1' $(-)$	**0.00**	0.13	1.00
R_2' $(-)$	0.52	**0.00**	1.00

Table 5.6: Comparison of R_1' and R_2' for the experimental tests [4].

$K = 0.1$ bar^2 gave the lowest R_1', meaning that this gain gave the lowest sum of pumping pressure changes [4]. The controller steadily increased the pumping pressure

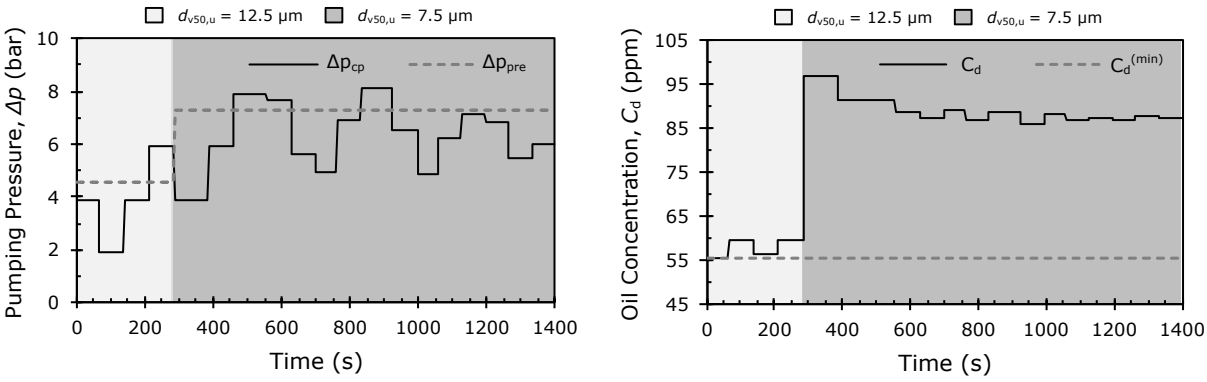

Figure 5.15: Experimental testing of the BVSS P&O-algorithm with $K = 100$ bar^2 [4].

toward the predicted optimum in steps of the minimum size, demonstrating that having too low gain makes the variable step size controller act as a constant step size controller [4]. $K = 10$ bar^2 gave a slightly higher R_1' compared to $K = 0.1$ bar^2, meaning that bigger pumping pressure steps were introduced [4]. However, $K = 10$ bar^2 resulted in the lowest R_2', meaning that this gain gave the lowest total sum of oil downstream of the hydrocyclone [4]. $K = 100$ bar^2 resulted in the highest value of both R_1' and R_2', indicating that this gain was too high [4]. Further details and discussions of the results are found in [4].

5.4.2 Tracking failure

Figure 5.16 shows simulations of the BVSS P&O-algorithm. The left plot is an adapted version of Figure 5 in [4] and shows the controller stepping in the correct direction after the environmental change. The right plot is an adapted version of Figure 10 in [4], showing the algorithm stepping away from, rather than toward, the new optimal point of operation. Both plots show two simulations, one having a controller gain $K = 0.1$ bar^2 (gray line) and the other having $K = 10$ bar^2 (black line). The dotted line is the model predicted optimal pumping pressure, included as a reference.

Comparing the two simulations having $K = 10$ bar^2, it is seen that the stepping direction is related to the direction of the previous step [4]. For the studied case, the environmental change reduced the size of the upstream oil droplets, consequently reducing the hydrocyclone separation efficiency and increasing the optimal pumping pressure. This increased the oil concentration downstream of the hydrocyclone, making the P&O-algorithm step in the opposite direction of the previous step, regardless of whether it was approaching the new optimum or not [4]. Compared to the results having $K = 0.1$ bar^2, it is seen that the variable step size only has an advantage if the system steps in the correct direction [4]. In the right plot, the system having $K = 0.1$ bar^2 made just a small step astray before turning toward the predicted optimal pumping pressure, whereas the

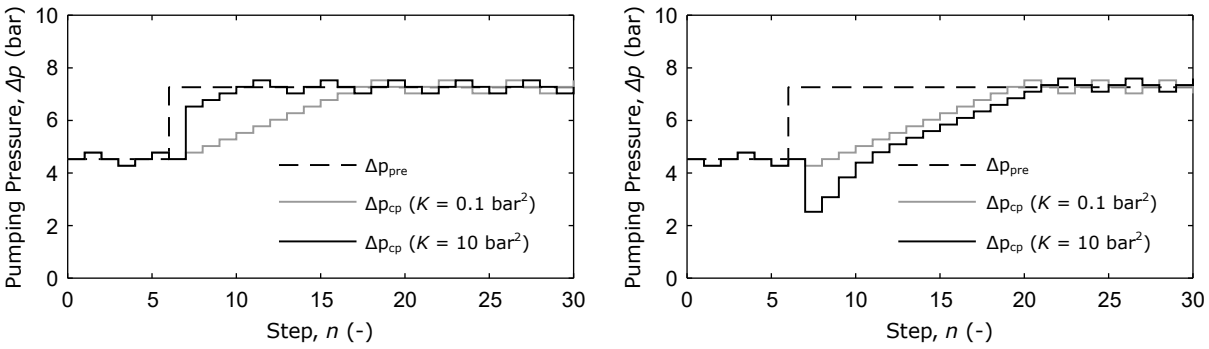

Figure 5.16: Left: Simulation of the BVSS P&O-algorithm stepping in the correct direction [4]. Right: Simulation of the BVSS P&O-algorithm stepping astray [4].

simulation with $K = 10$ bar^2 had to compensate for the large step astray.

5.4.3 Probe step and dormant mode

Two extended variable step size P&O-algorithms were developed, which avoids stepping astray by first introducing a probe step to determine in which direction to make the primary step. The two extended algorithms were called the hybrid variable step size (HVSS) P&O-algorithm, and the triggered variable step size (TVSS) P&O-algorithm. The following is an introduction to the principle of each the algorithm. Further details and schematics can be found in [4].

Figure 5.17 shows adapted versions of Figure 12 and Figure 14 in [4]. The figure contains two plots, where the left plot is a simulation of the HVSS P&O-algorithm and the right plot shows a simulation of the TVSS P&O-algorithm. In both simulations, the controller gain was $K = 10$ bar^2, and the predicted optimal pumping pressure is added as a reference.

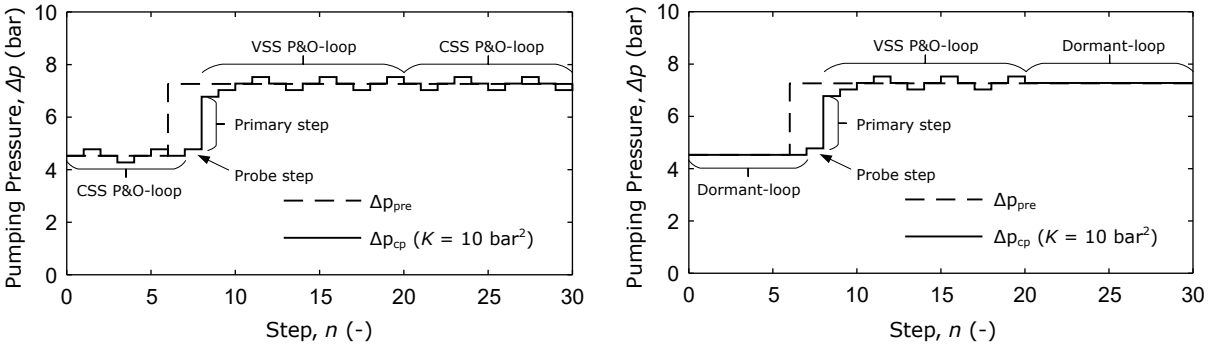

Figure 5.17: Left: Simulation of the HVSS P&O-algorithm [4]. Right: Simulation of the TVSS P&O-algorithm [4].

The HVSS P&O-algorithm starts off in what is called the constant step size (CSS)

P&O-loop, encircling the current optimal pumping pressure with a constant step size. When an abrupt change in the downstream oil concentration is detected, the HVSS P&O-algorithm introduces a probe step. The probe step is a minimum sized step and is used to determine whether the new optimal pumping pressure is higher or lower compared to the current point of operation. Next, the routine introduces a primary step in the direction determined based on the probe step. The size of the primary step is determined by the impact of the environmental change, using Eq. 5.4. After the primary step, the HVSS P&O-algorithm enters a variable step size (VSS) P&O-loop, in which it stays until the routine has switched from incrementing to decrementing the pumping pressure, or vice versa, for more than a predetermined number of times. When the predetermined number of directional changes has been reached, it is assumed that the new optimal point of operation has been found. Therefore, the routine returns to the CSS P&O-loop, continuing to encircle the optimal pumping pressure in small steps until a new significant change occurs [4].

The TVSS P&O-algorithm works similarly, but instead of entering a CSS P&O-loop when having reached the optimal point of operation, the TVSS P&O-algorithm enters a dormant-loop. In the dormant loop, the point of operation is kept constant until the current downstream oil concentration differs from the value it had when the algorithm first entered the loop, by more than a predetermined amount. This may happen either through abrupt changes or by gradual drifting. When the variation in downstream oil concentration has reached the limit, the TVSS P&O-algorithm performs the same probe step, primary step and variable step size routine as the HVSS P&O-algorithm, only to return to a constant point of operation rather than a constant step size loop when the optimal point of operation has been reached [4].

To determine which algorithm to implement, the constant steady-state pumping pressure of the TVSS P&O-algorithm must be weighed against the continuous tracking of the HVSS P&O-algorithm for the particular case the tracking is to be implemented [4].

Chapter 6

Conclusions

This thesis successfully shows that the novel coalescing centrifugal pump can be actively controlled to maximize the efficiency of downstream produced water treatment equipment, using real-time process information and tracking techniques.

Throughout this project:

- A once-through test rig has been designed and built, allowing for experimental testing using model oil and stabilized crude oil.
- The coalescing performance of the novel pump has been investigated and modeled based on experimental testing and droplet formation theory.
- The characteristics and benefits of combining the coalescing pump with a deoiling hydrocyclone have been investigated and modeled based on experimental testing, and droplet formation and separation theory.
- P&O-algorithms for actively controlling the pump and to continuously track the optimal point of operation have been developed, implemented, and demonstrated.
- The continuous tracking techniques have been compared to a model-prediction method, optimizing the pump operation based on upstream process information.
- Constant step size P&O-algorithms, used to track optimal pump operation, have been improved by introducing a variable step size and routines to avoid tracking failure.

In total, this project has resulted in a unique and novel utilization of emerging pump technology. Concerning operational control, the coalescing pump has been innovatively combined with existing produced water treatment equipment, utilizing the potential of the pump to maximize the treatment efficiency.

6.1 Outlook

As the portion of produced water increases, and fields are kept in operation for extended periods of time, a holistic perspective will be required to minimize the content of dispersed oil and other environmentally harmful substances in the effluent produced water, and to reach the zero-discharge goal. Not only treatment technologies should be included in this perspective, but also the produced water management system as a whole. For instance, continuous monitoring throughout the process plant can allow for performance optimization and identification of sub-optimal processing sections.

As exemplified in this thesis, real-time monitoring can be used in active control strategies, optimizing the performance of the process plant and reducing the discharge of oil and environmentally harmful substances. Such tracking strategies may be adopted by other droplet-size sensitive produced water treatment technologies, e.g., gravitational, enhanced gravitational, and flotation technologies, in addition to filter technologies and applications yet to be discovered. Also, applications not directly linked to produced water treatment may be considered, e.g., oil continuous flow applications and gas dehydration.

6.2 Further work

In a continuation of this project, an important step will be to implement the considered control strategies in an actual produced water treatment plant for verification. The implementation will allow for the identification of situations and operating conditions not considered in the present work, and, subsequently, for adaption and improvement of the control strategies.

Further studies of the droplet formation processes taking place inside of the novel coalescing pump should also be conducted. Such studies could include the development of mechanistic models predicting the effluent droplet size distribution. In combination with models of the downstream separation equipment, these mechanistic models may be used to predict the real-time optimal point of operation for varying operational conditions. The models may also be used during design or re-design of new and existing process plants, and to size and predict the performance of pumps and downstream separation equipment more accurately.

Bibliography

[1] R. Husveg, T. Husveg, N. van Teeffelen, M. Ottestad, and M. R. Hansen. Performance of a Coalescing Multistage Centrifugal Produced Water Pump with Respect to Water Characteristics and Point of Operation. In *Proc. of the Produced Water Workshop*, Aberdeen, United Kingdom, June 2016.

[2] R. Husveg, T. Husveg, N. van Teeffelen, M. Ottestad, and M. R. Hansen. Improving Separation of Oil and Water With a Novel Coalescing Centrifugal Pump. *SPE Production & Operations*, Preprint, 2018. SPE-188772-PA.

[3] R. Husveg, T. Husveg, N. van Teeffelen, M. Ottestad, and M. R. Hansen. Automatic Operation and Control of a Novel Coalescing Centrifugal Pump for Improved Oil/Water Separation. Manuscript submitted for publication, 2018.

[4] R. Husveg, T. Husveg, N. van Teeffelen, M. Ottestad, and M. R. Hansen. Variable Step Size P&O Algorithms for Coalescing Pump/Deoiling Hydrocyclone Produced Water Treatment System. Manuscript submitted for publication, 2018.

[5] A. Fakhru'l-Razi, A. Pendashteh, L. C. Abdullah, D. R. A. Biak, S. S. Madaeni, and Z. Z. Abidin. Review of technologies for oil and gas produced water treatment. *Journal of Hazardous Materials*, 170(2–3):530–551, October 2009.

[6] J. M. Walsh. The Savvy Separator Series: Part 5. The Effect of Shear on Produced Water Treatment. *Oil and Gas Facilities*, 5(1):16–23, February 2016. SPE-0216-0016-OGF.

[7] J. C. Ditria and M. E. Hoyack. The Separation of Solids and Liquids With Hydrocyclone-Based Technology for Water Treatment and Crude Processing. In *Proc. of the SPE Asia Pacific Oil and Gas Conference*, Melbourne, Australia, November 1994. SPE-28815-MS.

[8] M. T. Thew. Cyclones for oil/water separation. In *Encyclopedia of Separation Science*, pages 1480–1490. Academic Press, 2000.

[9] N. van Teeffelen. Development of a New Separation Friendly Centrifugal Pump. Presented at TEKNA Produced Water Management, Stavanger, Norway, 2015.

[10] OSPAR. Recommendation 2001/1 for the Management of Produced Water from Offshore Installations, 2001.

[11] J. A. Veil, M. G. Puder, D. Elcock, and R. J. Redweik Jr. A white paper describing produced water from production of crude oil, natural gas, and coal bed methane. Technical report, Argonne National Laboratory, United States, January 2004.

[12] S. Judd, H. Qiblawey, M. Al-Marri, C. Clarkin, S. Watson, A. Ahmed, and S. Bach. The size and performance of offshore produced water oil-removal technologies for reinjection. *Separation and Purification Technology*, 134:241–246, September 2014.

[13] DNV GL. Utredning av beste tilgjengelige teknikker for rensing av produsert vann som slippes ut fra petroleumsvirksomheten til havs. Technical Report 2015-0992, Rev. 01, Miljødirektoratet, 2015. [In Norwegian].

[14] E. T. Igunnu and G. Z. Chen. Produced water treatment technologies. *International Journal of Low-Carbon Technologies*, 9(3):157–177, September 2014.

[15] DNV GL. Håndtering av produsert vann - erfaringer fra norsk sokkel. Technical Report 2015-4277, Rev. 0, Norsk olje og gass, 2015. [In Norwegian].

[16] Miljødirektoratet. Arbeid mot nullutslipp til sjø fra petroleumsvirksomhet offshore, status 2016 [Report on the work towards the zero discharge goal on discharges to sea in the petroleum offshore sector]. Technical Report M-643, Miljødirektoratet, 2016. [In Norwegian].

[17] J. M. Walsh. Produced-Water-Treatment Systems: Comparison of North Sea and Deepwater Gulf of Mexico. *Oil and Gas Facilities*, 4(2):73–86, April 2015. SPE-159713-PA.

[18] N. Kharoua, L. Khezzar, and Z. Nemouchi. Hydrocyclones for De-oiling Applications—A Review. *Petroleum Science and Technology*, 28(7):738–755, April 2010.

[19] T. Husveg. *Operational Control of Deoiling Hydrocyclones and Cyclones for Petroleum Flow Control*. PhD thesis, University of Stavanger, 2007.

[20] N. Meldrum. Hydrocyclones: A Solution to Produced-Water Treatment. *SPE Production Engineering*, 3(4):669–676, November 1988. SPE-16642-PA.

[21] M. S. Choi. Hydrocyclone Produced Water Treatment for Offshore Developments. In *Proc. of the SPE Annual Technical Conference and Exhibition*, New Orleans, Louisiana, September 1990. SPE-20662-MS.

[22] S. M. Stroder and E. E. Wolfenberger. Hydrocyclone Separation: A Preferred Means of Water Separation and Handling in Oilfield Production. In *Proc. of the Permian Basin Oil and Gas Recovery Conference*, Midland, Texas, March 1994. SPE-27671-MS.

[23] M. Jiang, L. Zhao, J. He, and F. Zhou. Pressure Drop Ratio – An Important Performance Parameter In Liquid-Liquid Hydrocyclone Separation. In *Proc. of the Eighth International Offshore and Polar Engineering Conference*, Montreal, Canada, May 1998. ISOPE-I-98-150.

[24] Z. Yang, S. Pedersen, and P. Durdevic. Cleaning the Produced Water in Offshore Oil Production by Using Plant-wide Optimal Control Strategy. In *Proc. of the 2014 Oceans - St. John's*, St. John's, NL, Canada, September 2014.

[25] Z. Yang, P. Durdevic, and S. Pedersen. Optimization of Offshore De-oiling Hydrocyclone Performance: Plant-wide Control and Real-time OiW Measurement. In *Proc. of the Produced Water Workshop*, Aberdeen, United Kingdom, June 2016.

[26] D. A. Flanigan, J. E. Stolhand, M. E. Scribner, and E. Shimoda. Droplet Size Analysis: A New Tool for Improving Oilfield Separations. In *Proc. of the SPE Annual Technical Conference and Exhibition*, Houston, Texas, October 1988. SPE-18204-MS.

[27] D. A. Flanigan, J. E. Stolhand, E. Shimoda, and F. Skilbeck. Use of Low-Shear Pumps and Hydrocyclones for Improved Performance in the Cleanup of Low-Pressure Water. *SPE Production Engineering*, 7(3):295–300, August 1992. SPE-19743-PA.

[28] M. F. Schubert. Advancements in Liquid Hydrocyclone Separation Systems. In *Proc. of the Offshore Technology Conference*, Houston, Texas, May 1992. OTC-6869-MS.

[29] J. M. Walsh and T. C. Frankiewicz. Treating Produced Water on Deepwater Platforms: Developing Effective Practices Based Upon Lessons Learned. In *Proc. of the SPE Annual Technical Conference and Exhibition*, Florence, Italy, September 2010. SPE-134505-MS.

[30] A. Nocente. *Separation Friendly Produced Water Pumps.* PhD thesis, Norwegian University of Science and Technology, 2016.

[31] M. F. Almi, H. Belmili, M. Arrouf, and B. Bendib. A NOVEL ADAPTIVE VARIABLE STEP SIZE P&O MPPT ALGORITHM. *Academic Journal of Science*, 6(1):533–540, December 2016.

[32] J. P. Ram, T. S. Babu, and N. Rajasekar. A comprehensive review on solar PV maximum power point tracking techniques. *Renewable and Sustainable Energy Reviews*, 67:826–847, January 2017.

[33] A. Sachan, A. K. Gupta, and P. Samuel. A Review of MPPT Algorithms Employed in Wind Energy Conversion Systems. *Journal of Green Engineering*, 6(4):385–402, September 2017.

[34] B. R. Peng, J. H. Chen, Y. H. Liu, and Y. H. Chiu. Comparison between Three Different Types of Variable Step-Size P&O MPPT Technique. In *Proc. of the International Conference on Computer Information Systems and Industrial Applications*, Bangkok, Thailand, June 2015.

[35] A. K. Gupta and R. Saxena. Review on widely-used MPPT Techniques for PV Applications. In *Proc. of the 2016 International Conference on Innovation and Challenges in Cyber Security*, Noida, India, February 2016.

[36] About OSPAR. `https://www.ospar.org/about`. Accessed: 2018-06-05.

[37] Role and area of responsibility. `http://www.ptil.no/role-and-area-of-responsibility/category916.html`. Accessed: 2018-06-05.

[38] Petroleum Safety Authority Norway. Regulations Relating to Conducting Petroleum Activities (The Activities Regulations), 2017.

[39] OSPAR. Recommendation 2012/5 for a risk-based approach to the Management of Produced Water Discharges from Offshore Installations, 2012.

[40] Miljøverndepartementet. St. meld. nr. 58 (1996-97) Miljøvernpolitikk for en bærekraftig utvikling - Dugnad for framtida., 1997. [In Norwegian] `https://www.regjeringen.no/no/dokumenter/st-meld-nr-58_1996-97/id191317/`.

[41] S. Johnsen, T. K. Frost, M. Hjelsvold, and T. R. Utvik. The Environmental Impact Factor - a proposed tool for produced water impact reduction, management and regulation. In *Proc. of the SPE International Conference on Health, Safety and Environment in Oil and Gas Exploration and Production*, Stavanger, Norway, June 2000. SPE-61178-MS.

[42] H. Rye, M. Reed, M. K. Ditlevsen, S. Berntsen, and E. Garpestad. The "Environment Impact Factor" (EIF) for Produced Water Discharges – A Tool for Reducing Environmental Impacts. In *Development and Application of Computer Techniques to Environmental Studies X*, pages 23–32. WIT Press, 2004.

[43] M. Yang. Measurement of Oil in Produced Water. In *Produced Water*, pages 57–88. Springer, 2011.

[44] OSPAR. Agreement 2005/15 Reference Method of Analysis for the Determination of the Dispersed Oil Content in Produced Water, 2005.

[45] National Measurement System. An Introduction to Produced Water Management, 2011.

[46] OSPAR. Background Document concerning Techniques for the Management of Produced Water from Offshore Installations, 2013.

[47] M. Nasiri, I. Jafari, and B. Parniankhoy. Oil and Gas Produced Water Management: A Review of Treatment Technologies, Challenges, and Opportunities. *Chemical Engineering Communications*, 204(8):990–1005, July 2017.

[48] S. Jiménez, M. M. Micó, M. Arnaldos, F. Medina, and S. Contreras. State of the art of produced water treatment. *Chemosphere*, 192:186–208, February 2018.

[49] H. Devold. *Oil and Gas Production Handbook - An Introduction to Oil and Gas Production, Transport, Refining and Petrochemical industry.* ABB Oil and Gas, Oslo, Norway, 3.0 edition, August 2013.

[50] D. E. Leng and R. V. Calabrese. Immiscible Liquid-Liquid Systems. In *Handbook of Industrial Mixing: Science and Practice*, pages 639–754. John Wiley & Sons, Inc., 2004.

[51] Y. Liao and D. Lucas. A literature review of theoretical models for drop and bubble breakup in turbulent dispersions. *Chemical Engineering Science*, 64(15):3389–3406, August 2009.

[52] M. J. van der Zande. *Droplet break-up in turbulent oil-in-water flow through a restriction.* PhD thesis, Delft University of Technology, 2000.

[53] Y. Liao and D. Lucas. A literature review on mechanisms and models for the coalescence process of fluid particles. *Chemical Engineering Science*, 65(10):2851–2864, May 2010.

[54] Malvern Instruments Ltd. *RTSizer and Insitec analyser User Manual*, 2010.

[55] G. O. Brown. The History of the Darcy-Weisbach Equation for Pipe Flow Resistance. In *Proc. of the ASCE Civil Engineering Conference and Exposition*, Washington, D.C., November 2002.

[56] T. Husveg, T. Bilstad, P. G. A. Guinée, J. Jernsletten, B. Knudsen, and H. T. Nordbø. A Cyclone-Based Low Shear Valve for Enhanced Oil-Water Separation. In *Proc. of the Offshore Technology Conference*, Houston, Texas, May 2009. OTC-20029-MS.

[57] R. Morales, E. Pereyra, S. Wang, and O. Shoham. Droplet Formation Through Centrifugal Pumps for Oil-in-Water Dispersions. *SPE Journal*, 18(1):172–178, December 2012. SPE-163055-PA.

[58] R. Dabirian, S. Cui, I. Gavrielatos, R. Mohan, and O. Shoham. Evaluation of Models for Droplet Shear Effect of Centrifugal Pump. In *Proc. of the ASME 2018 Join US-European Fluids Engineering Summer Conference*, Montreal, Quebec, Canada, July 2018.

[59] J. O. Hinze. Fundamentals of the hydrodynamic mechanism of splitting in dispersion processes. *A.I.Ch.E. Journal*, 1(3):289–295, September 1955.

[60] S. Hall, M. Cooke, A. El-Hamouz, and A. J. Kowalski. Droplet break-up by in-line Silverson rotor–stator mixer. *Chemical Engineering Science*, 66(10):2068–2079, May 2011.

[61] H. Lamb. *Hydrodynamics*. Cambridge University Press, 6 edition, 1975.

[62] A. F. Sayda and J. H. Taylor. Modeling and Control of Three-Phase Gravity Separators in Oil Production Facilities. In *Proc. of the 2007 American Control Conference*, New York, July 2007.

[63] W. M. G. T. van den Broek, R. Plat, and M. J. van der Zande. Comparison of Plate Separator, Centrifuge and Hydrocyclone. In *Proc. of the SPE International Oil and Gas Conference and Exhibition in China*, Beijing, China, November 1998. SPE-48870-MS.

[64] Z. I. Khatib. Handling, Treatment, and Disposal of Produced Water in the Offshore Oil Industry. In *Proc. of the SPE Annual Technical Conference and Exhibition*, New Orleans, Louisiana, September 1998. SPE-48992-MS.

[65] D. A. Colman and M. T. Thew. CORRELATION OF SEPARATION RESULTS FROM LIGHT DISPERSION HYDROCYCLONES. *Chemical Engineering Research and Design*, 61:233–240, July 1983.

[66] T. Husveg. Centrifugal pump with coalescing effect, design method and use thereof, November 2015. Patent US 2015/0337842 A1.

[67] Turner Designs Hydrocarbon Instruments. *TD-500D User Manual*, 2015.